A dual-pathway architecture enables chronic stress to promote habit formation

Jacqueline R. Giovanniello[1], Natalie Paredes[1], Anna Wiener[1], Kathia Ramírez-Armenta[1], Chukwuebuka Oragwam[1], Hanniel O. Uwadia[1], Kayla Lim[2], Gift Nnamdi[1], Alicia Wang[1], Megha Sehgal[1], Fernando MCV Reis[1], Ana C. Sias[1], Alcino J. Silva[1,3,4], Avishek Adhikari[1,3,4], Melissa Malvaez[1], Kate M. Wassum[1,3,4]

[1]Dept. of Psychology, UCLA, Los Angeles, CA 90095. [2]Dept. of Biological Chemistry, UCLA, Los Angeles, CA 90095. [3]Brain Research Institute, UCLA, Los Angeles, CA 90095, USA. [4]Integrative Center for Learning and Memory, University of California Los Angeles, Los Angeles, CA, USA.

Correspondence:
Kate Wassum: kwassum@ucla.edu
Dept. of Psychology, UCLA
1285 Franz Hall
Box 951563
Los Angeles, CA 90095-1563

Key words: learning, decision making, instrumental conditioning, basolateral amygdala, central amygdala, reward, striatum

Figures: 4
Tables: 0
Supplemental Figures: 13
Supplemental Tables: 5
Words:
Abstract: 166
Main Text: 3551

ABSTRACT

Chronic stress can change how we learn and, thus, how we make decisions by promoting the formation of inflexible, potentially maladaptive, habits. Here we investigated the neuronal circuit mechanisms that enable this. Using a multifaceted approach in male and female mice, we reveal a dual pathway, amygdala-striatal, neuronal circuit architecture by which a recent history of chronic stress shapes learning to disrupt flexible goal-directed behavior in favor of inflexible habits. Chronic stress inhibits activity of basolateral amygdala projections to the dorsomedial striatum to impede the action-outcome learning that supports flexible, goal-directed decisions. Stress also increases activity in direct central amygdala projections to the dorsomedial striatum to promote the formation of rigid, inflexible habits. Thus, stress exerts opposing effects on two amygdala-striatal pathways to promote premature habit formation. These data provide neuronal circuit insights into how chronic stress shapes learning and decision making, and help understand how stress can lead to the disrupted decision making and pathological habits that characterize substance use disorders and other psychiatric conditions.

When making a decision, we can use what we have learned about our actions and their outcomes to prospectively evaluate the consequences of our potential choices[1-3]. This goal-directed strategy supports our agency. It allows us to choose actions that lead to desirable consequences and avoid those that lead to outcomes that are not currently beneficial. This strategy is, thus, highly flexible to changing circumstances. But we don't always think about the consequences of our behavior. Often this is fine. Such habits are a way for our brain to efficiently execute routine behaviors based on past success, without forethought of their consequences[4,2,5-7]. The brain balances goal-directed and habitual control to allow behavior to be adaptive when needed, yet efficient when appropriate[8,9]. But disrupted goal-directed control and overreliance on habit can cause inadequate consideration of consequences, inflexible behavior, a lower threshold for compulsivity, and disrupted decision making[10-13]. This can contribute to cognitive deficits in numerous diseases, including substance use disorder[14-25], obsessive-compulsive disorder[26-28], obesity[12,21,29], schizophrenia[30-32], depression[31,33], anxiety[34], and autism[35]. Chronic stress tips the balance of behavioral control towards habit[36-60]. Stress can change how we learn and, thus, how we make decisions, promoting inflexible habits. Because stress is a major predisposing factor for addiction and other psychiatric conditions[61-66], understanding how stress promotes habit formation will illuminate one avenue of vulnerability for these conditions. Yet, despite importance for understanding adaptive and maladaptive behavior, little is known of the neuronal circuits that enable stress-potentiated habit formation.

Amygdala-striatal projections are potential candidate pathways by which stress could bias learning and behavioral control strategy. The dorsomedial striatum (DMS) is an evolutionarily conserved hub for the action-outcome learning that supports goal-directed behavioral control[4,67-75]. Suppression of DMS activity prevents goal-directed control and promotes inflexible habits[70,76]. The basolateral amygdala (BLA) is needed for goal-directed behavior[77-79] and sends a direct excitatory projection to the DMS[80-86]. We know very little of the function of the BLA→DMS pathway, though it is well-positioned to facilitate the action-outcome learning that supports goal-directed behavior. Conversely, the central amygdala (CeA) has been implicated in habit[79]. It sends a direct, likely inhibitory[87,88], projection to the striatum[80,81]. No function for this newly identified CeA→striatum pathway has yet to be reported but these projections are poised to oppose DMS function. Both the BLA and CeA are highly implicated in stress processing[89-92]. Thus, here we investigated whether chronic stress acts via these amygdala-striatal pathways to promote habit formation.

RESULTS

Chronic stress potentiates habit formation

We first designed a behavioral procedure to model stress-potentiated habit formation in male and female mice (Figure 1a). Mice received 14 consecutive days of chronic mild unpredictable stress (CUS) including daily exposure to 2 of 6 stressors of variable duration at pseudorandom times and order: damp bedding (4-16 hrs), tilted cage (4-16 hr), white noise (80 db; 2-16 hr), continuous illumination during the dark phase (12 hr), physical restraint (2 hr), footshock (0.7-mA, 1-s, 5 shocks/10 min). We selected this stress protocol to model aspects of the repeated and varied nature of stress experienced by humans, including uncontrollable physical aversive events, disrupted sleep, and poor environmental conditions. Controls received equated handling. Demonstrating efficacy, serum

corticosterone levels were elevated (Figure 1b) and body weight was reduced (Figure 1c) in stressed mice relative to controls. This procedure was intentionally mild to model low-level chronic stress. Accordingly, it did not cause major anxiety- or depression-like phenotypes in classic assays of such behavior (Figure 1-1). 24 hours following the last stressor, mice were trained to lever press to earn a food-pellet reward. We used a random-ratio schedule of reinforcement to encourage action-outcome learning and goal-directed behavioral control[8,93-96]. Mice were food-deprived for training and, thus, bodyweight did not differ between control and stressed mice during training (Supplemental Table 1). Control and stressed mice similarly acquired the instrumental behavior (Figure 1d). Thus, CUS does not cause general learning, motivational, or locomotor impairments. To evaluate behavioral control strategy, we used the gold-standard outcome-specific devaluation test[2-4,7,67,97-100]. Mice were given 90-min, non-contingent access to the food pellet earned during training to induce a sensory-specific satiety rendering that specific food pellet temporarily devalued. Lever pressing was assessed in a 5-min, non-reinforced probe test immediately following the prefeeding. Performance was compared to that following satiation on an alternate food pellet to control for general satiety (Valued state; test order counterbalanced). Both control and stressed mice consumed similar amounts during the prefeed (Supplemental Table 2), indicating that CUS did not alter food consumption. CUS also did not affect outcome discrimination or devaluation efficacy. Both groups rejected the devalued outcome in a post-probe consumption choice test (Supplemental Table 3). If subjects have learned the action-outcome relationship and are using this to support prospective consideration of action consequences for flexible, goal-directed behavioral control, they will reduce lever pressing when the outcome is devalued relative to the valued state. We saw this effect in control subjects (Figure 1e-f; see also Supplemental Figure 1-2 for data on entries into the food-delivery port). Behavior in stressed mice was insensitive to devaluation, indicating the lack of consideration of action consequences that marks inflexible habits[4,7,8,67,97]. Thus, a recent history of chronic stress causes premature habit formation.

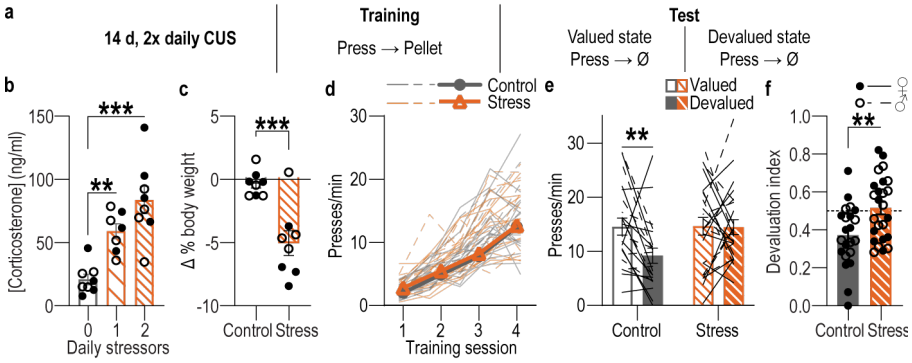

Figure 1: A recent history of chronic stress potentiates habit formation. (a) Procedure schematic. CUS, chronic unpredictable mild stress. Valued state = prefed on untrained food-pellet type to control for general satiety. Devalued state = prefed on trained food-pellet type to induce sensory-specific satiety devaluation. **(b)** Blood serum corticosterone concentrations 24 hr after completion of 14 d of 1 stressor/d, 2 stressors/d, or daily handling (Control). Stress: $F_{(2, 20)} = 17.35$, $P < 0.0001$. Control: N = 8 (4 male), 1x CUS: N = 7 (3 male), 2x CUS: N = 8 (4 male). **(c)** Percent change (Δ) in body weight averaged across the first 10 d of CUS on ad libitum food. $t_{14} = 4.50$, $P = 0.0005$. N = 8/group (4 male). **(d)** Press rate across training following CUS (Stress) or daily handling control. Training: $F_{(2.12, 95.32)} = 168.20$, $P < 0.0001$; Stress: $F_{(1, 45)} = 0.64$, $P = 0.43$, Training x Stress: $F_{(3, 135)} = 0.15$, $P = 0.93$. **(e)** Press rate during the subsequent devaluation probe test immediately following sensory-specific satiety devaluation of the trained pellet (Devalued) or an alternate pellet type (Valued). Stress x Value: $F_{(1, 45)} = 4.43$, $P = 0.04$; Stress: $F_{(1, 45)} = 2.52$, $P = 0.12$; Value: $F_{(1, 45)} = 4.88$, $P = 0.03$. **(f)** Devaluation index [(Devalued condition presses)/(Valued condition presses + Devalued presses)]. $t_{(45)} = 2.99$, $P = 0.005$. Control N = 22 (13 male), Stress N = 25 (12 male). Males = closed circles/solid lines, Females = open circles/dashed lines. $^{**}P < 0.01$, $^{***}P < 0.001$.

Chronic stress attenuates BLA→DMS and engages CeA→DMS pathway activity during learning.

We next confirmed the existence of direct BLA[80-86] and CeA[80,81] projections to dorsal striatum using both anterograde and retrograde tracing. We found that like the BLA, the CeA also directly projects the DMS (Supplemental Figure 2). We then characterized the activity of the BLA→DMS and CeA→DMS pathways during action-outcome learning and asked whether it is influenced by a recent history of chronic stress. We used fiber photometry to record fluorescent activity of the genetically encoded calcium indicator GCaMP8s expressed using an intersectional approach in either BLA or CeA neurons that project to the DMS (Figure 2a, b, d, j). Mice received 14 consecutive days of CUS or daily handling control prior to being trained to lever press to earn a food-pellet reward, as above (Figure 2c). Again, both control and stressed mice similarly acquired the instrumental behavior (Figure 2e, k, see also Figure 2-1 for food-port entry data). Fiber photometry (473 nm calcium-dependent, 415 nm isosbestic) recordings were made during each training session. BLA→DMS neurons were robustly activated by the earned reward during learning (Figure 2f-i). Thus, the BLA→DMS pathway is active when subjects are able to learn the rewarding consequence of their actions and form the action-outcome memories that support goal-directed behavioral control. This activity was absent in stressed mice (Figure 2g). Thus, recent chronic stress attenuates BLA→DMS activity associated with action-outcome learning. Conversely, CeA→DMS neurons are not robustly active during this form of instrumental learning, but chronic stress engages this pathway particularly around earned reward experience later in training (Figure 2l-o). Thus, chronic stress recruits the CeA→DMS pathway to instrumental learning. We detected similar patterns in response to unpredicted rewards in both pathways (Figure 2-2). Both BLA→DMS and CeA→DMS projections were acutely activated by unpredicted footshock and this was not altered by stress (Figure 2-2), providing a positive control for our ability to detect signal in all groups. This also indicates that neither BLA→DMS nor CeA→DMS activity is valence-specific. Chronic stress did, however, reduce post-shock activity in the BLA→DMS pathway, consistent with its effects on reward signals in this pathway. Chronic stress did not alter baseline spontaneous calcium activity in either pathway, indicating it does not generally increase or decrease excitability in these pathways (Figure 2-3). Together these data indicate that a recent history of chronic stress oppositely modulates BLA→DMS and CeA→DMS projections during learning, turning off learning-related activity in the BLA→DMS pathway and instead engaging the CeA→DMS pathway.

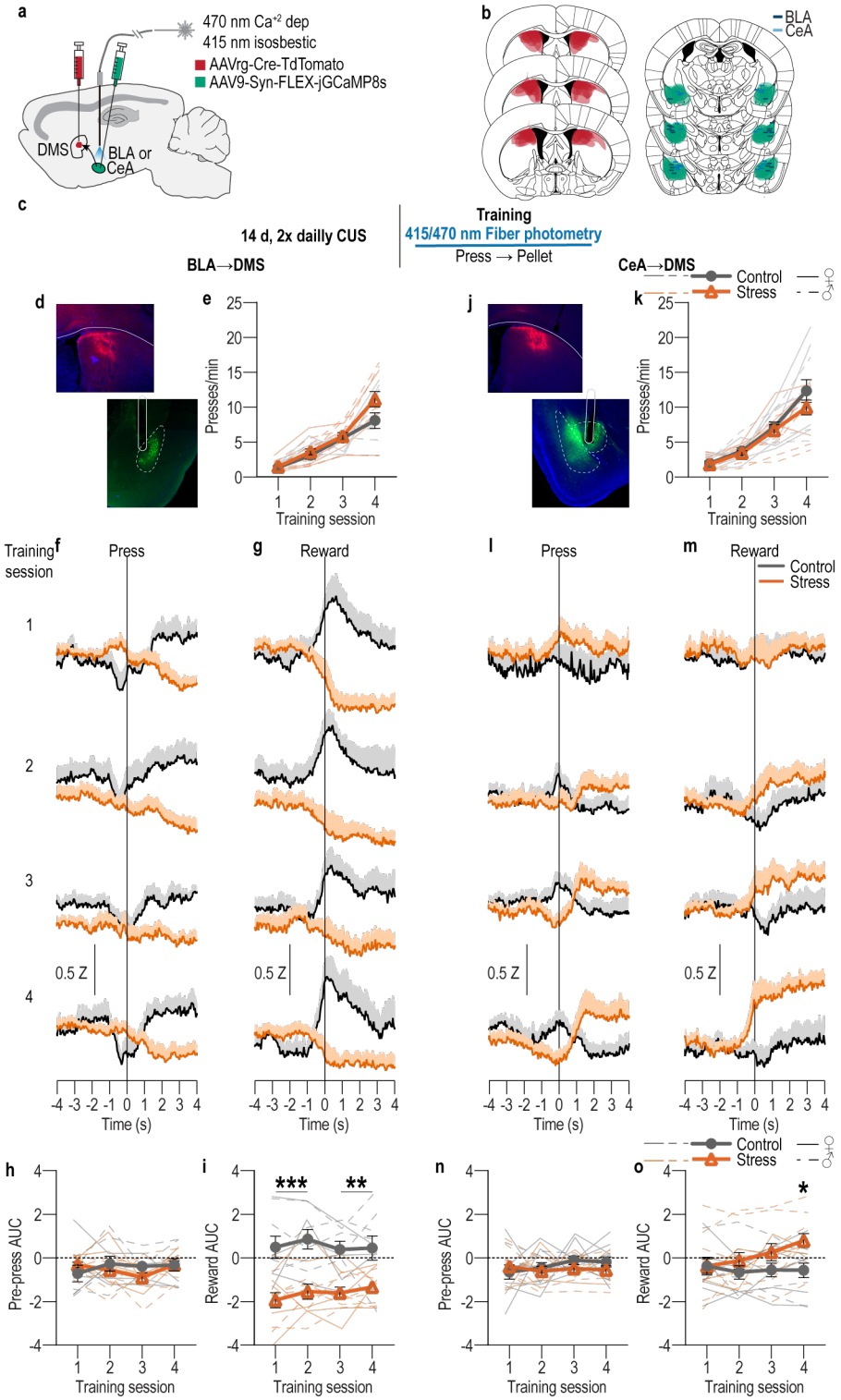

Figure 2: Chronic stress attenuates BLA→DMS and engages CeA→DMS pathway activity during instrumental learning. (a) Intersectional approach for fiber photometry calcium imaging of DMS-projecting BLA or CeA neurons. **(b)** Schematic representation of retrograde AAV-cre in DMS and cre-dependent GCaMP8s expression and optical fiber tips in BLA or CeA for all subjects. **(c)** Procedure schematic. CUS, chronic unpredictable stress. **(d-i)** Fiber photometry recordings of GCaMP8s in BLA→DMS neurons during instrumental lever press – food-pellet reward learning. **(d)** Representative images of retro-cre expression in DMS and immunofluorescent staining of cre-dependent GCaMP8s expression and fiber placement in BLA. **(e)** Press rate across training following CUS (Stress) or daily handling control. Training: $F_{(1.72,\ 32.66)} = 81.40$, $P < 0.0001$; Stress: $F_{(1,\ 19)} = 2.25$, $P = 0.15$; Training x Stress: $F_{(3,\ 57)} = 3.19$, $P = 0.03$. **(f-g)** Trial-averaged Z-scored Δf/F BLA→DMS GCaMP8s fluorescence changes aligned to bout-initiating presses (f; first press of the session and first press after a reward collection) and reward collection (g; first food-port entry after reward delivery) across each training session. **(h-i)** Trial-averaged quantification of area under the BLA→DMS GCaMP8s Z-scored Δf/F curve (AUC) during the 3-s period prior to initiating presses (h; Training: $F_{(2.49,\ 47.38)} = 0.91$, $P = 0.43$; Stress: $F_{(1,\ 19)} = 0.18$, $P = 0.68$; Training x Stress: $F_{(3,\ 57)} = 1.77$, $P = 0.16$) or following reward collection (i; Stress: $F_{(1,\ 19)} = 24.13$, $P < 0.0001$; Training: $F_{(2.41,\ 45.71)} = 0.91$, $P = 0.43$; Training x Stress: $F_{(3,\ 57)} = 0.78$, $P = 0.51$) across training. Control N = 9 (4 male), Stress N = 12 (5 male). **(j-o)** Fiber photometry recordings of GCaMP8s in CeA→DMS neurons

during instrumental lever press – food-pellet reward learning. **(j)** Representative immunofluorescent image of retro-cre expression in DMS and cre-dependent GCaMP8s expression and fiber placement in CeA. **(k)** Press rate across training following CUS (Stress) or daily handling control. Training: $F_{(1.51, 30.23)} = 65.61$, $P < 0.0001$; Stress: $F_{(1, 20)} = 1.106$, $P = 0.31$; Training x Stress: $F_{(3, 60)} = 1.05$, $P = 0.38$. **(l-m)** Trial-averaged Z-scored Δf/F CeA→DMS GCaMP8s fluorescence changes aligned to bout-initiating presses (l) and reward collection (m) across each training session. **(n-o)** Trial-averaged quantification of CeA→DMS GCaMP8s Z-scored Δf/F AUC during the 3-s period prior to initiating presses (n; Training: $F_{(2.36, 47.26)} = 0.60$, $P = 0.58$; Stress: $F_{(1, 20)} = 0.74$, $P = 0.40$; Training x Stress: $F_{(3, 60)} = 0.92$, $P = 0.44$) or following reward collection (o; Training x Stress: $F_{(3, 60)} = 4.51$, P = 0.006; Training: $F_{(2.34, 46.75)} = 3.23$, $P = 0.04$; Stress: $F_{(1, 20)} = 2.41$, $P = 0.14$). Control N = 11 (6 male), Stress N = 11 (4 male). Males = closed circles/solid lines, Females = open circles/dashed lines. *P <0.05, **P <0.01, ***P < 0.001.

Suppression of BLA→DMS pathway activity disrupts action-outcome learning and enables chronic stress to promote habit formation

We next reasoned that the stress-induced suppression of BLA→DMS projection activity during action-outcome learning might promote premature habit formation. We tested this by asking whether activating BLA→DMS projections during instrumental learning is sufficient to restore goal-directed behavioral control in stressed mice. Using an intersectional approach (Figure 3a), we expressed the excitatory designer receptor human M3 muscarinic receptor (hM3Dq) or fluorophore control in DMS-projecting BLA neurons (Figure 3b-c). Following 14 consecutive days of CUS or daily handling control, mice received instrumental training to lever press to earn food-pellet rewards (Figure 3d). Prior to each training session, mice received the hM3Dq ligand clozapine-N-oxide (CNO; 0.2 mg/kg[101-104] i.p.) to activate BLA→DMS projections during learning. Neither stress nor chemogenetic activation of BLA→DMS projections altered acquisition of the instrumental lever-press behavior (Figure 3e; see also Figure 3-1 for food-port entry data). Whereas controls were sensitive to subsequent outcome devaluation, indicating action-outcome learning and goal-directed behavioral control, stressed mice were, again, insensitive to devaluation, indicating premature habit formation (Figure 3f-g). Chemogenetic activation of BLA→DMS projections during learning restored normal action-outcome learning enabling goal-directed behavioral control, as evidenced by sensitivity to devaluation, in stressed mice (Figure 3f-g; see Figure 3-2 for effects of chemogenetic BLA→DMS activation in handled controls). Thus, activation of BLA→DMS projections during learning is sufficient to overcome the effect of prior chronic stress and restore action-outcome learning for flexible, goal-directed behavioral control.

Given that BLA→DMS projections are activated by earned rewards during learning, we next reasoned that this activity might be critical for the action-outcome learning that supports goal-directed behavioral control. If this is true, then inhibiting reward-evoked BLA→DMS activity should suppress action-outcome learning and prematurely promote habit formation in mice without a history of chronic stress. To test this, we used pathway-specific optogenetic inhibition of BLA→DMS activity at the time of earned reward during action-outcome learning. We expressed the inhibitory opsin archaerhodopsin (Arch) or fluorophore control in the BLA and implanted optical fibers in the DMS in the vicinity of Arch-expressing BLA axons and terminals (Figure 3h-j). We used green light (532 nm, 10 mW, 5 s) to inhibit BLA terminals in the DMS during collection of each earned reward during instrumental lever press - food pellet training (Figure 3k). BLA→DMS inhibition did not affect acquisition of the instrumental behavior (Figure 3l; see also Figure 3-1 for food-port entry data), but did disrupt action-outcome learning as evidenced by subsequent insensitivity to outcome devaluation at test (Figure 3m-n). BLA→DMS inhibition was not inherently rewarding or aversive (Figure 3-3). Thus, BLA→DMS projections are normally

activated by rewarding events to enable the action-outcome learning that supports flexible, goal-directed behavior. Chronic stress turns off this activity to disrupt action-outcome learning and promote premature habit formation.

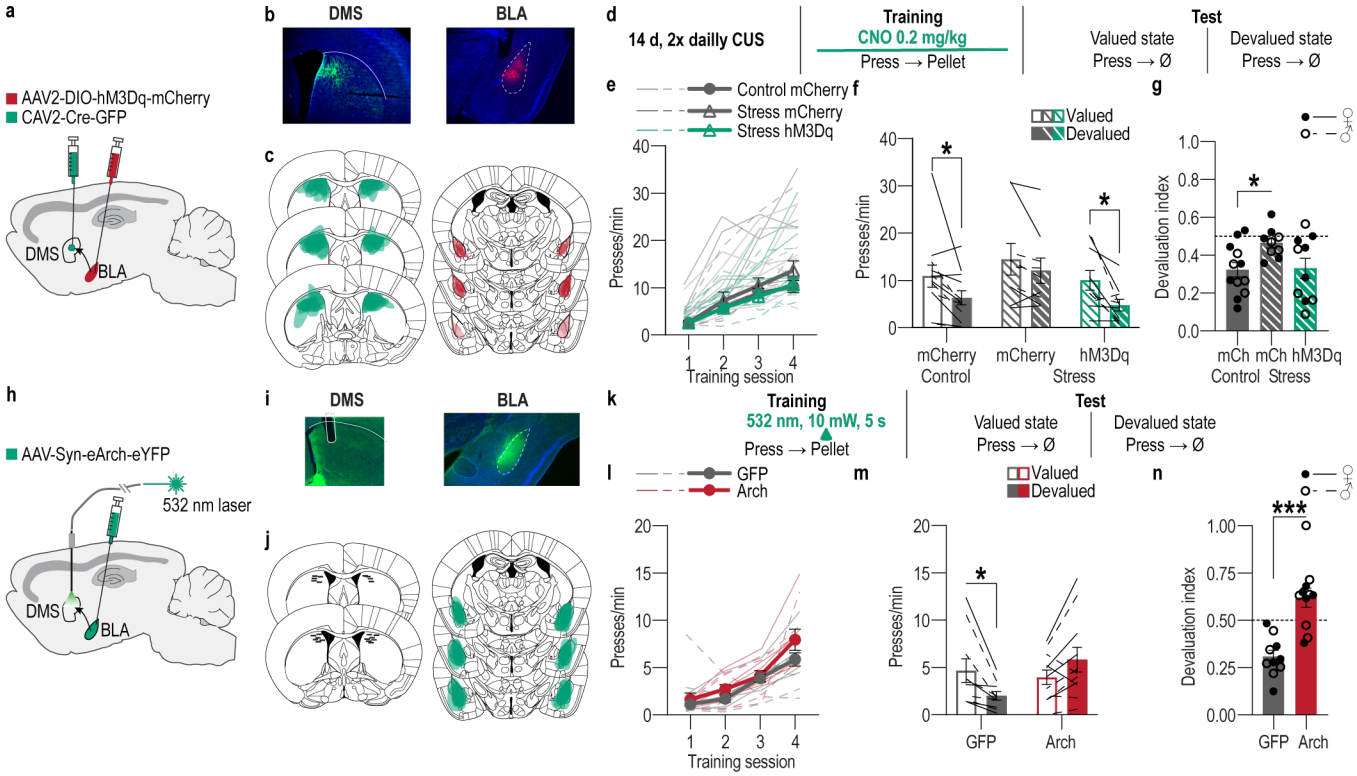

Figure 3: Suppression of BLA→DMS pathway activity disrupts action-outcome learning and enables chronic stress to promote habit formation. (a-g) Chemogenetic activation of BLA→DMS projections during post-stress instrumental learning. **(a)** Intersectional approach for chemogenetic activation of DMS-projecting BLA neurons. **(b)** Representative immunofluorescent images of retro-cre expression in DMS and cre-dependent hM3Dq expression in BLA. **(c)** Schematic representation of retro-cre in DMS and cre-dependent hM3Dq expression in BLA for all subjects. **(d)** Procedure schematic. CUS, chronic unpredictable stress. CNO, clozapine-N-oxide. Valued state = prefed on untrained food-pellet type to control for general satiety. Devalued state = prefed on trained food-pellet type to induce sensory-specific satiety devaluation. **(e)** Press rate across training following CUS (Stress) or daily handling control. Training: $F_{(1.90, 53.30)}$ = 60.55, P < 0.0001; Group: $F_{(2, 28)}$ = 1.05, P = 0.36; Training x Group: $F_{(6, 84)}$ = 0.80, P = 0.57. **(f)** Press rate during the subsequent devaluation probe test immediately following sensory-specific satiety devaluation of the trained pellet (Devalued) or an alternate pellet type (Valued). Value: $F_{(1, 28)}$ = 18.07, P = 0.0002; Group: $F_{(2, 28)}$ = 2.06, P = 0.15; Group x Value: $F_{(2, 28)}$ = 0.75, P = 0.48. **(g)** Devaluation index [(Devalued condition presses)/(Valued condition presses + Devalued presses)]. Group: $F_{(2, 28)}$ = 3.38, P = 0.048. Control mCherry N = 12 (7 male), Stress mCherry N = 9 (5 male), Stress hM3Dq N = 10 (5 male). **(h-n)** Optogenetic inactivation of BLA→DMS projections at reward during instrumental learning. **(h)** Approach for optogenetic inhibition of BLA terminals in DMS. **(i)** Representative immunofluorescent images of Arch expression in BLA and optical fiber tip in the vicinity of Arch-expression BLA terminals in the DMS. **(j)** Schematic representation of Arch expression in BLA and approximate location of optical fiber tips in DMS for all subjects. **(k)** Procedure schematic. **(l)** Press rate across training. Training: $F_{(1.70, 32.34)}$ = 41.26, P < 0.0001; Virus: $F_{(1, 19)}$ = 2.43, P = 0.14; Training x Virus: $F_{(3, 57)}$ = 1.14, P = 0.34. **(m)** Press rate during the subsequent devaluation probe test immediately following sensory-specific satiety devaluation of the trained pellet (Devalued) or an alternate pellet type (Valued). Stress x Value: $F_{(1, 19)}$ = 14.35, P = 0.001; Stress: $F_{(1, 19)}$ = 1.43, P = 0.25; Value: $F_{(1, 19)}$ = 0.43, P = 0.52. **(n)** Devaluation index. $t_{(19)}$ = 5.03, P < 0.0001. GFP N = 10 (5 male), Arch N = 11 (5 male). Males = closed circles/solid lines, Females = open circles/dashed lines. *P <0.05, ***P <0.001.

Chronic stress engages the CeA→DMS pathway to promote habit formation

As opposed to the BLA→DMS pathway, chronic stress engages the CeA→DMS pathway during learning. We reasoned that this, too, may be a mechanism through which stress promotes premature habit formation. If this is true, then preventing the stress-induced increase in CeA→DMS activity during learning should restore action-outcome learning and goal-directed behavioral control. We tested this in two ways. First, we used an intersectional approach (Figure 4a) to express the inhibitory designer receptor human M4 muscarinic receptor

(hM4Di), or a fluorophore control in DMS-projecting CeA neurons (Figure 4b-c). Following 14 consecutive days of CUS or daily handling control, mice received instrumental training to lever press to earn food-pellet rewards (Figure 4d). Prior to each training session, mice received the hM4Di ligand clozapine-N-oxide (CNO; 2.0 mg/kg[105-107] i.p.) to inactivate CeA→DMS projections during learning. Neither stress nor chemogenetic inactivation of CeA→DMS projections altered acquisition of the instrumental behavior (Figure 4e; see also Figure 4-1 for food-port entry data). At test, we again found evidence of goal-directed behavioral control, sensitivity to devaluation, in control subjects and potentiated habit formation, insensitivity to devaluation, in stressed subjects (Figure 4f-g). Chemogenetic inhibition of CeA→DMS projection activity during learning restored action-outcome learning to enable goal-directed behavioral control, sensitivity to devaluation, in stressed mice (Figure 4f-g).

Chronic stress engages the CeA→DMS pathway specifically at reward experience during learning. Therefore, we next asked whether this stress-induced CeA→DMS reward response is necessary for premature habit formation, by optogenetically inhibiting CeA terminals in the DMS at the time of earned reward during learning in stressed mice. We expressed the inhibitory opsin Arch or fluorophore control in the CeA and implanted optical fibers in the DMS in the vicinity of Arch-expressing CeA axons and terminals (Figure 4h-j). Following 14 days of CUS or daily handling control, mice received instrumental training to lever press to earn food-pellet rewards (Figure 4k). We used green light (532 nm, 10 mW, 5 s) to inhibit CeA terminals in the DMS during the collection of each earned reward (Figure 4k). Neither stress nor optogenetic inhibition of CeA→DMS projection activity in stressed subjects altered acquisition of the instrumental behavior (Figure 4l; see also Figure 4-1 for food-port entry data). Similar to chemogenetic inhibition, optogenetic inhibition of CeA→DMS activity at reward during learning restored action-outcome learning to enable goal-directed behavioral control in stressed mice, as evidenced by sensitivity to devaluation (Figure 4m-n). Neither chemogenetic nor optogenetic inhibition of CeA→DMS projections altered learning or subsequent behavioral control strategy in mice without a history of chronic stress (Figure 4-2). Thus, chronic stress engages CeA→DMS projections during subsequent reward learning experience to promote premature habit formation.

We next used pathway-specific optogenetic stimulation to ask whether CeA→DMS pathway activity at reward during learning is sufficient to promote premature habit formation. We used an intersectional approach (Figure 4a) to express the excitatory opsin Channelrhodopsin 2 (ChR2) or a fluorophore control in DMS-projecting CeA neurons and implanted optic fibers above the CeA (Figure 4o-q). We first used blue light (473 nm, 10 mW, 20 Hz, 25-ms pulse width, 2 s) to stimulate CeA→DMS neurons during the collection of each earned reward during instrumental learning in mice without a history of chronic stress. This neither affected acquisition of the lever-press behavior, nor the action-outcome learning needed to support flexible, goal-directed behavioral control during the devaluation test (Figure 4-3). Thus, activation of the CeA→DMS pathway during reward learning experience is not alone sufficient to disrupt action-outcome learning or promote habit formation. We next asked whether activation of CeA→DMS projections is sufficient to amplify the effects of a less frequent prior chronic stress experience on habit formation. We repeated the experiment this time in mice with a history of once daily CUS for 14 consecutive days (Figure 4r). Again, neither CeA→DMS activation nor stress altered acquisition of

the instrumental behavior (Figure 4s; see Figure 4-1 for food-port entry data). The less frequent chronic stress was itself insufficient to cause premature habit formation, but when coupled with activation of CeA→DMS projections at reward during learning did cause premature habit formation as evidenced by greater insensitivity to devaluation in subjects that received stimulation relative to those that did not (Figure 4t-u). Thus, activation of CeA→DMS projections during learning is sufficient to amplify the effects of prior subthreshold chronic stress to promote habit formation. CeA→DMS stimulation was not found to be inherently rewarding or aversive in either control or stressed subjects (Figure 4-4). Together, these data indicate that chronic stress recruits the CeA→DMS pathway to subsequent learning to promote the premature formation of inflexible habits.

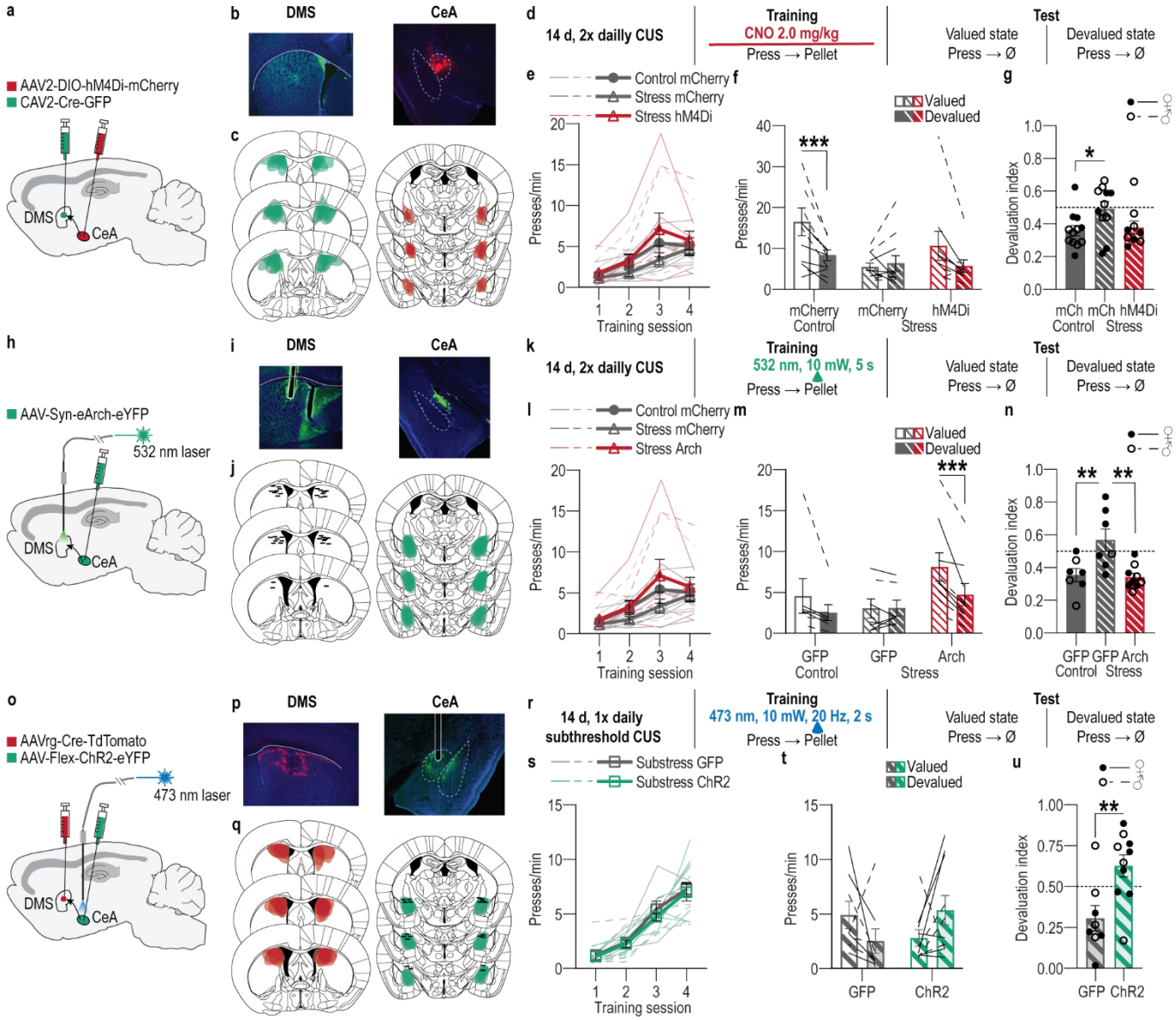

Figure 4: Chronic stress engages the CeA→DMS pathway to promote habit formation. (a-g) Chemogenetic inhibition of CeA→DMS projections during post-stress instrumental learning. **(a)** Intersectional approach for chemogenetic inhibition of DMS-projecting CeA neurons. **(b)** Representative immunofluorescent images of retro-cre expression in DMS and cre-dependent hM4Di expression in CeA. **(c)** Schematic representation of retro-cre in DMS and cre-dependent hM4Di expression in CeA for all subjects. **(d)** Procedure schematic. CUS, chronic unpredictable stress. CNO, clozapine-N-oxide. Valued state = prefed on untrained food-pellet type to control for general satiety. Devalued state = prefed on trained food-pellet type to induce sensory-specific satiety devaluation. **(e)** Press rate across training following CUS (Stress) or daily handling control. Training: $F_{(1.46, 42.19)} = 12.57$, $P = 0.0002$; Group: $F_{(2, 29)} = 0.23$, $P = 0.79$; Training x Group: $F_{(6, 87)} = 0.59$, $P = 0.74$. **(f)** Press rate during the subsequent devaluation probe test immediately following sensory-specific satiety devaluation of the trained pellet (Devalued) or an alternate pellet type (Valued). Group x Value: $F_{(2, 29)} = 5.85$, $P = 0.007$; Value: $F_{(1, 29)} =$

12.86, P = 0.001; Group: $F_{(2, 29)}$ = 2.65, P = 0.09. **(g)** Devaluation index [(Devalued condition presses)/(Valued condition presses + Devalued presses)]. Group: $F_{(2, 29)}$ = 3.59, P = 0.04. Control mCherry N = 12 (5 male), Stress mCherry N = 11 (5 male), Stress hM4Di N = 9 (4 male). **(h-n)** Optogenetic inactivation of CeA→DMS projections at reward during post-stress learning. **(h)** Approach for optogenetic inhibition of CeA terminals in DMS. **(i)** Representative immunofluorescent images of Arch expression in CeA and optical fiber tip in the vicinity of Arch-expressing CeA terminals in the DMS. **(j)** Schematic representation of Arch expression in BLA and approximate location of optical fiber tips in DMS for all subjects. **(k)** Procedure schematic. **(l)** Press rate across training following CUS (Stress) or daily handling control. Training: $F_{(1.80, 36.14)}$ = 22.71, P < 0.0001; Group: $F_{(2, 20)}$ = 0.93, P = 0.41; Training x Group: $F_{(6, 60)}$ = 1.67, P = 0.34. **(m)** Press rate during the subsequent devaluation probe test immediately following sensory-specific satiety devaluation of the trained pellet (Devalued) or an alternate pellet type (Valued). Group x Value: $F_{(2, 20)}$ = 4.25, P = 0.03; Value: $F_{(1, 20)}$ = 13.66, P = 0.001; Group: $F_{(2, 20)}$ = 1.74, P = 0.20. **(n)** Devaluation index. Group: $F_{(2, 20)}$ = 7.81, P = 0.003. Control GFP N = 7 (4 male), Stress GFP N = 7 (6 male), Stress Arch N = 9 (5 male). **(o-u)** Optogenetic stimulation of CeA→DMS projections at reward during learning following subthreshold chronic stress. **(o)** Intersectional approach for optogenetic stimulation of DMS-projecting CeA neurons. **(p)** Representative images of retro-cre expression in DMS and immunofluorescent staining of cre-dependent ChR2 expression in CeA. **(q)** Schematic representation of retro-cre in DMS and cre-dependent ChR2 expression in CeA for all subjects. **(r)** Procedure schematic. **(s)** Press rate across training following once/daily, 14 d CUS. Training: $F_{(2.11, 33.69)}$ = 76.17, P < 0.0001; Virus: $F_{(1, 16)}$ = 0.33, P = 0.57; Training x Virus: $F_{(3, 48)}$ = 0.19, P = 0.90. **(t)** Press rate during the subsequent devaluation probe test immediately following sensory-specific satiety devaluation of the trained pellet (Devalued) or an alternate pellet type (Valued). Virus x Value: $F_{(1, 16)}$ = 4.56, P = 0.049; Virus: $F_{(1, 16)}$ = 0.09, P = 0.76; Value: $F_{(1, 16)}$ = 0.004, P = 0.95. **(u)** Devaluation index. $t_{(16)}$ = 3.12, P = 0.007. GFP N = 8 (4 male), ChR2 N = 10 (6 male). Males = closed circles/solid lines, Females = open circles/dashed lines. ns = not significant. *P <0.05, **P < 0.01, ***P <0.001.

DISCUSSION

These data reveal a dual pathway neuronal circuit architecture by which a recent history of chronic stress shapes learning to disrupt flexible, goal-directed behavioral control in favor of inflexible habits. Both the BLA and CeA send direct projections to the DMS. The BLA→DMS pathway is activated by rewarding events and this mediates the action-outcome learning that supports flexible, goal-directed control of reward-seeking behavior. Chronic stress attenuates this activity to promote premature habit formation. Conversely, the CeA→DMS pathway is not robustly active during action-outcome learning, but stress recruits this pathway to promote premature habit formation. Thus, chronic stress promotes habit formation by altering the balance of BLA and CeA input to the DMS.

That the BLA→DMS pathway mediates action-outcome learning is consistent with evidence that BLA lesion disrupts goal-directed behavior[77-79] and BLA/DMS disconnection disrupts action-outcome learning[82]. Here we implicate direct BLA→DMS projections and show that this pathway is activated by rewarding events so one can link those rewards to the actions that earned them and, subsequently, use those action-outcome memories to engage in the prospective consideration of action consequences needed for flexible decision making. These data are, however, inconsistent with evidence that BLA→DMS ablation does not disrupt action-outcome learning[108]. Thus, temporally-specific manipulation was needed to reveal the function of this pathway in action-outcome learning. Chronic stress suppresses learning-related activity in BLA→DMS projections. This was surprising because the BLA is, generally, hyperactive following chronic stress[109-116] (c.f.[117]), but it indicates that chronic stress suppresses activity in the BLA pathway that is critical for the learning that supports flexible, goal-directed decision making. Given that the BLA→DMS projection is predominately excitatory[118-120], the BLA is poised to excite the DMS neuronal activity that mediates action-outcome learning[70-72,121-125]. Stress removes this influence to disrupt action-outcome learning and promote habit formation.

Like the BLA, we found that the CeA also targets the DMS. Unlike the BLA→DMS pathway, we find that the CeA→DMS pathway is not typically activated during action-outcome learning but is recruited by chronic stress to promote premature habit formation. This is consistent with evidence that the CeA is itself required for natural

habit formation[79]. It is also consistent with evidence that stress increases CeA activity[126-131]. Here we show that a recent history of chronic stress causes CeA→DMS projections to be activated by rewards during instrumental learning. This alters learning, disrupting the ability to engage in subsequent prospective consideration of action consequences in favor of inflexible, habitual behavioral control. Indeed, given that most CeA neurons are inhibitory[88,132], the recruitment of this pathway is poised to attenuate the DMS activity needed for action-outcome learning[70-72,121-123]. Previous work has shown that the CeA works indirectly, likely via the midbrain[133-136], with the dorsolateral striatum to regulate habit formation[79,137]. Thus, the CeA may promote habit learning through both direct and indirect pathways to the striatum. Whether stress acts via multiple CeA outputs to promote habit is a ripe question for future investigation. Interestingly, activation of the CeA→DMS pathway alone was not sufficient to recapitulate the effects of stress to promote habit formation. Rather CeA→DMS activation was sufficient to tip the balance towards habit following a subthreshold mild chronic stress experience. Thus, stress exposure may prime the CeA→DMS pathway to be recruited during subsequent learning. Additionally, CeA→DMS activation may work along with a confluence of disruptions, likely to the BLA→DMS pathway, but also to cortical inputs to DMS[60,123,138] and perhaps CeA outputs to midbrain[133,134], to promote habit formation.

These data support a parallel model[139] of amygdala function whereby, via distinct outputs to the DMS, the amygdala actively gates the nature of learning to regulate the balance of behavioral control strategies. Unlike valence-processing models of amygdala function[140,141], the data here indicate that BLA and CeA projections to DMS are unlikely to convey simple positive or negative valence, but rather differentially shape the content of learning. Chronic stress flips the balance of BLA and CeA inputs to the DMS to promote the formation of rigid, inflexible habits.

The discoveries here open the door to many important future questions. One is how prior chronic stress affects learning-associated BLA→DMS and CeA→DMS activity. That chronic stress occurred before training and did not alter spontaneous activity in either pathway, suggests that it may lay down neuroplastic changes in these pathways that become influential during subsequent learning opportunities. How such changes occur is a big and important question for future research. An equally substantial next question is how these pathways influence downstream DMS activity to promote habit formation. Indeed, DMS neuronal activity, especially plasticity in dopamine D1 receptor-expressing neurons[121], is critical for the action-outcome learning that supports goal-directed behavior[70-72,123] and when suppressed promotes inflexible habits[70,76]. A reasonable speculation is that the excitatory BLA→DMS pathway promotes downstream learning-related activity in DMS to support action-outcome learning and that the inhibitory CeA→DMS pathway dampens such activity to encourage habit formation. Amygdala-striatal inputs may coordinate in this regard with corticostriatal inputs, known to be important for supporting action-outcome learning[22,60,142]. The BLA→DMS and CeA→DMS pathways mediate the influence of stress on the learning that supports behavioral control strategies. Manipulations restricted to learning were sufficient to rescue normal goal-directed behavioral control following chronic stress. Whether these pathways similarly contribute to the expression of behavioral control strategies is also a ripe question for future investigation. Both amygdala subregions and DMS participate in drug-seeking[137,143-148] and active avoidance

behavior[149]. The central amygdala is particularly implicated in compulsive drug seeking and drug seeking after extended use, dependence and withdrawal, or stress[137,147,150,151]. Thus, more broadly, our results indicate chronic stress is poised to oppositely modulate BLA→DMS and CeA→DMS pathways to promote maladaptive drug-seeking and/or avoidance habits.

Adaptive decision making often requires understanding your agency in a situation. Knowing that your actions can produce desirable or undesirable consequences and using this to make thoughtful, deliberate, goal-directed decisions. Chronic stress can disrupt such agency and promote inflexible, habitual control over behavior. We found that stress does this with a one-two punch to the brain. Chronic stress dials down the BLA→DMS pathway activity needed to learn the association between an action and its consequence to enable flexible, well-informed decisions. It also dials up activity in the CeA→DMS pathway, causing the formation of rigid, inflexible habits. These data provide neuronal circuit insights into how chronic stress shapes how we learn and, thus, how we decide. This helps understand how stress can lead to the disrupted decision making and pathological habits that characterize substance use disorders and mental illness.

AUTHOR CONTRIBUTIONS

JRG and KMW conceptualized and designed the experiments, interpreted the data, and wrote the paper. JRG executed all experiments and analyzed the data. NP, AW, CO, HOU, GN assisted with experiments. MS assisted with rabies tracing experiments with resources from AJS. FMCVR assisted with RTPP experiments, with advice and resources from AA. ACS wrote initial code for photometry analysis. KRA analyzed spontaneous event frequency and amplitude on photometry data. MM contributed to the conceptualization and design of the experiments, initially optimized the instrumental conditioning procedures and data analysis, and provided important contributions to the interpretation of the data.

ACKNOWLEDGEMENTS

This research was supported by NIH R01DA046679 (KMW), NIH T32DA024635 (JRG), NIH F32DA056201 (JRG), A.P. Giannini Fellowship (JRG), NIH TL4GM118977 (NP), NIH R01MH119089 (AA), and the Staglin Center for Behavior and Brain Sciences. UCLA Behavioral Testing Core provided space and behavioral testing equipment for the open field, elevated plus maze and light-dark emergence test.

COMPETING FINANCIAL INTERESTS

The authors have no biomedical financial interests or potential conflicts of interest to declare.

METHODS

See Supplemental Table 5 for key reagents.

Subjects

Male and female wildtype C57/Bl6J mice (Jackson Laboratories, Bar Harbor, ME) aged 9-12 weeks old at the time of surgery served as subjects. Rabies tracing was conducted with *Drd1a-Cre* and *Adora2A-Cre* transgenic mice bred in house and aged 8-16 weeks at the time of surgery. Mice were housed in a temperature (68-79 °F) and humidity (30-70%) regulated vivarium on 12:12 hour reverse dark/light cycle (lights off at 7 AM). Behavioral experiments were performed during the dark phase. Mice were group housed in same-sex groups of 3-4 mice/cage prior to onset of behavioral experiments and subsequently single-housed for the remainder of the experiment to facilitate food deprivation and preserve implants. Unless noted below, mice were provided with food (standard rodent chow, Lab Diet, St. Louis, MO) and water *ad libitum* in the home cage. Mice were handled for 3-5 days prior to the start of behavioral training for each experiment. All procedures were conducted in accordance with the NIH Guide for the Care and Use of Laboratory Animals and were approved by the UCLA Institutional Animal Care and Use Committee.

Surgery

Mice were anesthetized with isoflurane (3% induction, 1% maintenance), and positioned in a digital stereotaxic frame (Kopf, Tujunga, CA). Subcutaneous Rimadyl (Carprofen; 5 mg/kg; Zoetis, Parsippany, NJ) was given pre-operatively for analgesia and anti-inflammatory purposes. Small cranial holes (1–2 mm^2) were drilled, through which virus or fluorescent tracers were delivered via a guide cannula (DMS: 28 ga, BLA/CeA: 33 ga), PlasticsOne, Roanoke, VA) connected to a 1-mL syringe (Hamilton Company, Reno, NV) by intramedic polyethylene tubing (BD; Franklin Lakes, NJ) and controlled by a syringe pump (Harvard Apparatus, Holliston, MA). Coordinates (from Bregma) were determined by mouse brain reference atlas[152] and were as follows: CeA, AP -1.2, ML ±2.8, DV -4.6 mm; BLA, AP -1.5, ML ±3.2, DV -5.0 mm; DMS, AP +0.2, ML ±1.8, DV -2.65 mm. Virus or tracers were infused at a rate of 0.1 µL/min and cannulae were left in place for at least 10 min post-injection. For injection-only surgeries, the skin was re-closed with Vetbond tissue adhesive (3M, Saint Paul, MN). For surgeries requiring fiber-optic cannulae, fibers were placed 0.3 mm above the target region for optogenetic experiments and at the infusion site for fiber photometry experiments, secured to the skull using RelyX Unicem Universal Self-Adhesive Resin (3M) and a head cap was created using C&B Metabond quick adhesive cement system (Parkell Inc., Brentwood, NY), followed by opaque dental cement (Lang Dental Manufacturing, Wheeling, IL). After surgery, mice were kept on a heating pad maintained at 35 °C for 1 hour and then single-housed in a new homecage for recovery and monitoring. Mice received chow containing the antibiotic TMS for 7 days following surgery to prevent infection, after which they were returned to standard rodent chow. Specific surgical details for each experiment are described below. In all cases, surgery occurred prior to the onset of stress and/or behavioral training.

Chronic mild unpredictable stress

The chronic mild unpredictable stress (CUS) procedure was modified from[60,153-156]. Mice assigned to the CUS group were exposed to 2 stressors/day (foot shock, physical restraint, tilted cage, white noise, continuous illumination, or damp bedding) for 14 days in a pseudorandomized manner at variable time onset and for varying durations between 2 and 16 hours. Control subjects received equated daily handling in the vivarium by the same experimenter administering the CUS. CUS was administered in a separate, enclosed laboratory space distinct from both the vivarium and behavioral testing rooms. CUS mice had home-cage nesting material removed for the duration of the CUS exposure[157]. Mice were transported to the stress space in individual 16-oz clear polyethylene containers and on a dedicated transport cart and placed into individual cages in the stress space. Stress efficacy was assessed by daily body weight measurements[158]. Sub-threshold CUS exposure was identical to CUS except mice received only 1 stressor/day.

Stressors

Footshock: Subjects were placed in the conditioning chamber for 2 min to acclimate and then exposed to 5, 2-3 s, 0.7-mA footshocks with a variable intertrial interval averaging 60 sec (30-90 sec range). The footshock chamber had a similar grid floor to the behavioral testing chambers (described below) but was otherwise distinct in wall shape (round), pattern (monochrome polka dot), lack of bedding, scent (75% ethanol), and lighting (off). The chambers also lacked food ports and levers. Chambers were cleaned with 75% ethanol between subjects.

Physical Restraint: Subjects were immobilized in modified 50-mL polypropylene conical tubes with 4 air holes per side, 1 at the top, and 1 in the cap for the tail (10 total). Mice were scruffed and placed inside the conical tube for 2 hours in their stress cage.

Tilted cage: Stress cages were placed on chocks to tilt each cage at approximately a 45-degree angle for 6 - 16 hours.

White noise: 100-db white noise was played in the stress space for all CUS mice for a duration of 6 - 16 hours.

Continuous illumination: Overhead lights were turned on during the dark phase of the light cycle (7PM – 7AM).

Damp bedding: ~200 mL of water was mixed with the stress cage corncob bedding. Mice were placed in their stress cage with this damp bedding for 6 - 16 hours. Mice were returned to a new home cage with clean, dry bedding afterwards.

Corticosterone ELISA

N = 11 male and *N* = 12 female mice were used for corticosterone measurements of blood serum after exposure to 0, 1, or 2 stressors per day for 14 day. Measurements were taken 24 hours after the final stress exposure. Mice were decapitated and trunk blood was collected in 1.7-mL sample tubes on ice. Tubes were centrifuged at 2000 g for 10 min at 4 °C. Clear supernatant was collected and placed in new 1.7-mL sample tubes and frozen at -20 °C. Samples were diluted 1:40 in sample dilution buffer. Serum corticosterone levels were assessed using a Corticosterone ELISA kit as directed (Enzo Biosciences; Farmingdale, NY) and quantified on a microplate reader (Molecular Devices, San Jose, CA).

Behavioral procedures

Instrumental conditioning and tests

Instrumental conditioning procedures were adapted from our prior work[97].

Apparatus. Training took place in Med Associates wide mouse conditioning chambers (East Fairfield, VT) housed within sound- and light-attenuating boxes. Each chamber had metal grid floors and contained a retractable lever to the left of a recessed food-delivery port (magazine) on the front wall. A photobeam entry detector was positioned at the entry to the food port. Each chamber was equipped with 2 pellet dispensers to deliver either 20-mg grain or chocolate-flavored purified pellets (Bio-Serv, Frenchtown, NJ) into the food port. A fan mounted to the outer chamber provided ventilation and external noise reduction. A 3-watt, 24-volt house light mounted on the top of the back wall opposite the food port provided illumination. To monitor subject behavior, monochrome digital cameras (Med Associates) were positioned over top of the conditioning chambers. For optogenetic manipulations, chambers were outfitted with an Intensity Division Fiberoptic Rotary Joint (Doric Lenses, Quebec, QC, Canada) connecting the output fiber optic patch cords to a 473-nm or 593-nm laser (Dragon Lasers, ChangChun, JiLin, China) positioned outside of the chamber.

Food deprivation. 3 - 5 days prior to the start of behavioral training, mice were food-deprived to maintain 85%-90% of their free-feeding body weight. Mice were given 1.5 - 3.0 g of their home chow at the same time daily at least 2 hours after training sessions. For experiments involving CUS, food deprivation began during the last 3 days of the stress procedure. Owing to food deprivation, body weights did not differ between groups at the start or end of training (see Supplemental Table 1).

Outcome pre-exposure. To familiarize subjects with the food pellet that would become the instrumental outcome, mice were given 1 session of outcome pre-exposure. Mice were placed in a clean, empty cage and allowed to consume 20 - 30 of the food pellets from a metal cup. If any pellets remained, they were placed in the home cage overnight for consumption.

Magazine conditioning. Mice received 1 session of training in the operant chamber to learn where to receive the food pellets (20-mg grain or chocolate-purified pellets). Mice received 20 - 30 non-contingent pellet deliveries from the food port with a fixed 60-s intertrial interval.

Instrumental conditioning. Mice received 4 sessions (1 session/day consecutively), minimum, of instrumental conditioning in which lever presses earned delivery of a single food pellet. Earned pellet type (grain or chocolate) was counterbalanced across subjects within each group of each experiment. Each session began with the illumination of the house light and extension of the lever, and ended with the retraction of the lever and turning off of the house light. Sessions ended after the total available outcomes (20 or 30, as noted for each experiment below) had been earned or a maximum time limit (20 or 30 min, as noted below) had been reached. In all cases, training began on a fixed-ratio 1 schedule (FR-1), in which each action was reinforced with one food pellet

outcome. Once mice completed 2 sessions in which they achieved 80% performance criteria (earned 80% of the max outcomes), the reinforcement schedule was escalated to either random interval (RI) or random ratio (RR) as described for each experiment below. For the RI protocol, mice received 1 session on an RI-15 s schedule then 2 - 3 sessions on the final RI-30 s schedule (variable average 15-s or 30-s interval must elapse following a reinforcer for another press to be reinforced). Subjects on the RR protocol received 1 session each of RR-2, RR-5, and RR-10 schedule of reinforcement (variable press requirement average of 2, 5, or 10 presses to earn the food pellet).

Alternate outcome exposures. To equate exposure of the non-trained pellet, all mice were given non-contingent access to same number of the alternate food pellets (e.g., chocolate pellets if grain pellets served as the training outcome) as the earned pellet type in a different context (clear plexiglass cage) a minimum of 2 hours before or after (alternated daily) each RI or RR instrumental training session.

Sensory-specific satiety outcome devaluation test. Testing began 24 hr after the final instrumental conditioning session. Mice were given 1 - 1.5 hours access to either 4 g of the food pellets previously earned by lever pressing (Devalued condition) or 4 g of the non-trained pellets to control for general satiety (Valued condition). The remaining pellets were weighed following prefeeding to measure total consumption. Consumption did not significantly differ between the Devalued v. Valued conditions for any experiment (Supplemental Table 2). Immediately after this prefeeding, lever pressing was assessed during a brief, 5-min, non-reinforced probe test. Following the probe test, mice were given a 10-min consumption choice test with simultaneous access to 1 g of both pellet types to ensure rejection of the devalued outcome. In all cases, mice consumed less of the prefed pellet than non-prefed pellet, indicating successful sensory-specific satiety devaluation (Supplemental Table 3). 24 hr after the first devaluation test, mice received 1 session of instrumental retraining on the final reinforcement schedule (RI30 or RR10), followed the next day by a second devaluation test in which they were prefed the opposite food pellet. Thus, each mouse was tested in both the Valued and Devalued conditions, with test order counterbalanced across subjects within each group for each experiment.

Real-time place preference/avoidance test

Procedure was conducted as described previously[159]. Mice were habituated to a 2-sided opaque plexiglass chamber (20 × 42 × 27 cm) for 10 min, during which their baseline preference for the left or right side of the chamber was measured. During the first 10-min test session, one side of the chamber was assigned to the light-delivery side (counterbalanced across subjects within each group). Mice were placed in the non-stimulation side to start the experiment. Light (Dragon Laser; Changchun, China) was delivered upon entry into the light-paired side and continued until the subject exited that side (optical stimulation: 473 nm, 5-ms pulse width, 20 Hz, ~8-10 mW at fiber tip; optical inhibition: 593 nm, continuous, ~8-10 mW). Mice then received a second test, identical to the first, in which the opposite side of the chamber served as the light-paired side. Sessions were video-recorded using a CCD camera. This camera interfaced with Biobserve software (Biobserve GmbH, Germany) and a Pulse Pal (Sanworks, Rochester, NY), to track subject position in real time and trigger laser delivery. The apparatus was cleaned with 75% ethanol after each session. Distance traveled, movement velocity, and time spent in each chamber was generated by Biobserve software post-session. Time spent in laser-paired chamber was compared between groups to assess preference or aversion of laser delivery.

Open-field test

Procedure was conducted as described previously[159]. Mice were placed in an opaque plexiglass arena (34 × 34 × 34 cm) for a single 10-min session. Sessions were video recorded using a CCD camera interfaced with Anymaze (Stoelting Co., Wood Dale, IL) software, which was used to track subject position in real time. Center region was defined as the innermost third of the floor area. Brightness above the OFT was ~70 lux. The apparatus was cleaned with 75% ethanol after each subject. Distance traveled, movement velocity, and time spent in either center or surrounding outer area was generated by Biobserve software and compared between groups.

Elevated plus maze

Procedure was conducted as described previously[160]. The dimensions of the elevated plus maze (EPM) arms were 30 cm x 7 cm, and the height of the closed arm walls was 20 cm. The maze was 65 cm elevated from the floor and was placed in the center of the behavior room away from other stimuli. Brightness above the EPM was ~70 lux. For the 10-min EPM test, mice were placed in the center of EPM facing a closed arm. Each session was video recorded using a CCD camera, which interfaced with Anymaze software to track subject location in real time. The apparatus was cleaned with 75% ethanol after each session. Distance traveled, movement

velocity, and time spent in the center, open arms, or closed arms was generated by Biobserve software and compared between groups.

Light/dark emergence test

The dark side of a 2-chamber apparatus was made of black opaque plexiglass and completely enclosed except for a small entry through the middle divider. The light side was made of white opaque plexiglass and was open to the light above. Brightness in the light chamber was ~70 lux. Mice were placed in the open portion of the apparatus to initiate a 10-min session. Each session was video recorded using a CCD camera, which interfaced with Anymaze software to track subject location. The apparatus was cleaned with 75% ethanol after each session. Distance traveled, movement velocity, and time spent in the light chamber was generated by Biobserve software and compared between groups.

Sucrose-preference test

Mice first received habituation to 2 standard home-cage water bottles filled with water in the home cage for 16 hours. Subsequently, one water bottle was replaced with a bottle of 10% sucrose. Bottles were left in place for 24 hours and weighed before and after placement. Bottle positions were switched for another 24-hour period and subsequently weighed again. Amount of sucrose and water consumed, as well as a ratio of the two, during the 48-hour period was compared between groups.

Progressive ratio test

Mice were trained on the instrumental training protocol above to a reinforcement schedule of RR-10. They were then given a progressive ratio test in which the number of lever presses required to receive a pellet increased by 4 with each reinforcer delivered (e.g., 1, 5, 9, 13, 17, 21 etc.). The session ended after >5-min break in pressing or maximum duration of 4 hr. Session duration, rewards delivered, total presses, and the break point (last completed press requirement) were collected and compared between groups.

Tracing

Anterograde tracing of CeA neurons was performed as previously described[161]. Male (*N* = 2) and female (*N* = 2) naïve mice were infused bilaterally with the anterograde tracer AAV8-Syn-mCherry (Addgene, Watertown, MA) in the CeA (0.2 µL). Virus was allowed to express for 4 weeks, following which mice were perfused and histology was processed as described below to identify fluorescently labeled fibers in the dorsal striatum.

For retrograde tracing of DMS-projecting amygdala neurons, male (*N* = 2) and female (*N* = 2) naïve mice were infused with Fluorogold (Sigma, St. Louis, MO; 4% in sterile saline) in the DMS (0.2 µL). Virus was allowed to express for 5 days, following which mice were perfused and histology was processed as described below to identify fluorescently labeled cell bodies in CeA and BLA.

For retrograde tracing of monosynaptic inputs onto Drd1a$^+$ or A2A$^+$ DMS neurons, male (*N* = 4) and female (*N* = 4) *Drd1a-cre* or male (*N* = 3) and female (*N* = 2) *Adora2A-cre* naïve mice were infused with 0.3 µL AAV2-hSyn-FLEX-TVA-P2A-eGFP-2A-oG (Salk Gene Transfer, Targeting and Therapeutics Facility) in the DMS. Three weeks later, mice were infused with 0.3 µL EnvA G-deleted Rabies-mCherry at the same DMS coordinates. Mice were perfused 1 week later and tissue was processed as described below to identify monosynaptically-labeled inputs in CeA and BLA. 4 *Drd1a-cre* and 1 *Adora2A-cre* subjects were removed due to starter virus spillover in the BNST.

Fiber photometry calcium imaging of CeA→DMS or BLA→DMS projections during instrumental learning following CUS

Male and female (CeA→DMS: *N* = 38, 14 male; BLA→DMS: *N* = 34, 13 male) naïve mice were used in this experiment to monitor calcium fluctuations in CeA→DMS and BLA→DMS projections during instrumental conditioning after CUS. 18 subjects with off-target viral expression and/or fiber location were excluded from the dataset. 4 subjects were excluded for loss of optic fibers/headcaps. 4 subjects were excluded for missing recording data from one session. 3 subjects that did not complete instrumental conditioning were also excluded. Mice were randomly assigned to Virus and Stress groups. At surgery, mice received unilateral infusion (left/right hemisphere counterbalanced across subjects within each group) of a retrogradely trafficked AAV encoding cre-recombinase (AAVrg-Syn-Cre-P2A-dTomato, Addgene) into the DMS (0.3 µl) and of an AAV encoding the cre-dependent genetically encoded calcium indicator GCaMP8s (AAV9-Syn-FLEX-GcAMP8s-GFP, Addgene) into either the CeA or BLA (0.1-0.2 µl). Optic fiber cannulae (5.0-mm length (BLA) or 4.6 mm (CeA), 200-µm diameter, 0.37 NA, Inper, Hangzhou, China) were implanted over the GCaMP infusion site for calcium imaging at cell

bodies. Mice were given 1 - 2 weeks to recover post-surgery, followed by 14 consecutive days of twice/daily CUS or daily handling as described above. Mice were habituated to restraint during the final 3 days of the CUS/handling period. 24 hours after the final CUS exposure, mice began instrumental conditioning as described above. Each session began with a 3-minute baseline period prior to the start of the instrumental session for assessment of changes in baseline calcium activity. After completion of FR-1, mice received 1 session each of training on an RR-2, RR-5, and RR-10 reinforcement schedule (max 20 outcomes/20 min/session). We chose an RR reinforcement schedule for this experiment because it tends to promote action-outcome learning and goal-directed behavioral control[94,95,100,123] and would, thus, make it more difficult for prior CUS to induce habits, increasing the robustness of the results.

Fiber photometry was used to image bulk calcium activity in CeA→DMS or BLA→DMS neurons for 3-min prior to and throughout each instrumental conditioning session using a commercial fiber photometry system (Neurophotometrics Ltd., San Diego, CA). Two light-emitting LEDs (470 nm: Ca^{2+}-dependent GCaMP fluorescence; 415 nm: autofluorescence, motion artifact, Ca^{2+}-independent GCaMP fluorescence) were reflected off dichroic mirrors and coupled via a patch cord (200 µm; 0.37 NA, Inper) to the implanted optical fiber. The intensity of excitation light was adjusted to ~100 µW at the tip of the patch cord. Fluorescence emission was passed through a 535-nm bandpass filter and focused onto the complementary metal-oxide semiconductor (CMOS) camera sensor through a tube lens. Samples were collected at 20 Hz interleaved between the 415 nm and 470 nm excitation channels using a custom Bonsai workflow. Time stamps of task events were collected simultaneously through an additional synchronized camera aimed at the Med Associates interface, which sent light pulses coincident with task events (onset, press, entry, reward). Signals were saved using Bonsai software and exported to MATLAB (MathWorks, Natick, MA) for analysis.

To assess the response to appetitive and aversive stimuli and provide a positive signal control, fiber photometry measurements were made during subsequent non-contingent reward and footshock sessions. In the first session, mice received 10 non-contingent food-pellet deliveries with a variable 60-s intertrial interval. 24 hours later, they received a session of 5, 2-s, 0.7mA footshocks with a variable 60-s intertrial interval. Calcium signal was aligned to reward collection or shock onset using timestamps collected as above. Mice were then perfused and brain tissue was processed with standard histology procedures described below to assess viral expression location/spread and fiber location.

Fiber photometry analysis

Data were pre-processed using a custom-written pipeline in MATLAB (MathWorks, Natick, MA) as previously[162]. The 415 nm and 470 nm signals were fit using an exponential curve. Change in fluorescence (ΔF/F) at each time point was calculated by subtracting the fitted 415 nm signal from the 470 nm signal and normalizing to the fitted 415 nm data [(470-fitted 415)/fitted 415)]. The ΔF/F data was Z-scored to the average of the whole session [(ΔF/F - mean ΔF/F)/std(ΔF/F)]. Z-scored traces were then aligned to behavioral event timestamps throughout each session. Area under the curve (AUC) was calculated for each individual aligned trace within each session using a trapezoidal function. We use the 3-s period prior to initiating presses to quantify activity related to the initiation of actions. We used the 3-s period following reward collection to quantify activity related to the earned outcome and unpredicted reward. We used the 1-s period following shock onset to quantify acute shock responses and the 2-s post-shock period to quantify activity following the shock. Quantifications and signal aligned to events were averaged across trials within a session and compared across sessions and between groups. Spontaneous activity was recorded during a 3-minute baseline period in the instrumental training context prior to each training session. Calcium events were identified as described previously[163]. First, we fitted the isosbestic channel to the 470 nm signal using an exponential function then subtracted the isosbestic trace from the calcium trace to remove calcium-independent artifacts. We defined a series of sliding-moving windows (15-s window, 1-second step) along the trace in which we filtered out high-amplitude events (greater than 2x the median of the 15-s window) and calculated the median absolute deviation of the resultant trace. Calcium transients with local maxima greater than 2 times above the median absolute deviation were selected as events. These events were used to calculate spontaneous event frequency and amplitude for BLA→DMS and CeA→DMS pathways.

Chemogenetic activation of BLA→DMS projections during instrumental learning following CUS

Male and female (mCherry *N* = 28, 14 male; hM3Dq: *N* = 26, 16 male) naïve mice were used in this experiment to assess whether activation of BLA→DMS projections during learning is sufficient to rescue action-outcome learning for goal-directed behavioral control in subjects with a history of CUS. 15 subjects with off-target viral expression and 2 subjects that did not complete instrumental conditioning were excluded from the dataset. Mice

were randomly assigned to Viral and Stress groups. At surgery, all mice received bilateral infusion of the retrogradely-trafficked canine-adenovirus encoding cre-recombinase (CAV2-Cre-GFP; Plateforme de Vectorologie de Montpellier, Montpellier, France) into the DMS (0.3 µl) and AAV encoding the cre-inducible excitatory designer receptor human M3 muscarinic receptor (hM3Dq; AAV2-Syn-DIO-hM3Dq-mCherry; Addgene, Watertown, MA) or fluorophore control (AAV2-Syn-DIO-mCherry; Addgene) into the BLA (0.1-0.2 µl). Mice were given 1-2 weeks to recover post-surgery, followed by 14 consecutive days of twice/daily CUS or daily handling, as described above. Mice were habituated to i.p. injections during the final 3 days of the CUS/handling period. 24 hours after the final CUS exposure, mice began instrumental conditioning, as described above. All subjects received an intraperitoneal (i.p.) injection of clozapine-*n*-oxide (water soluble CNO; 0.2 mg/kg[101-104,164]; Hello Bio, Princeton, NJ) 30 min prior to each instrumental conditioning session. Upon completion of FR-1 (80% max rewards delivered), mice received 1 training session the RI-15s reinforcement schedule following by 2 sessions on an RI-30s schedule (max 30 outcomes/30 min/session). We chose an RI schedule of reinforcement for this experiment because it tends to promote habit formation [94,95,100,123] and, thus, would make it more difficult to neurobiologically prevent stress-potentiated habit, increasing the robustness of the results. Following training mice received a counterbalanced pair of sensory-specific satiety outcome-specific devaluation tests, as above. No CNO was given on test days. CNO was given prior to the retraining session (RI-30s) in between tests. After instrumental training and testing, mice were perfused and brain tissue was processed using standard histology procedures described below to assess viral expression location and spread.

Optogenetic inhibition of BLA→DMS projections during instrumental learning

Male and female (eYFP *N* = 20, 10 male; Arch: *N* = 20, 10 male) naïve mice were used in this experiment to assess the necessity of BLA→DMS projection activity at outcome experience during training for the action-outcome learning that supports goal-directed behavioral control. 13 subjects with off-target viral expression or fiber location and 6 subjects that did not complete instrumental conditioning were excluded from the dataset. Mice were randomly assigned to Viral group. At surgery, mice received bilateral infusion of an AAV encoding the inhibitory opsin archaerhodopsin (AAVDJ-Syn-eArch-eYFP, Stanford Vector Core) or fluorophore control (AAV8-Syn-GFP; Addgene) into the BLA (0.1 - 0.2 µl). Optic fiber cannulae (2.4-mm length, 100-µm diameter, 0.22 NA, Inper) were implanted over the DMS. Mice were given 3 weeks to recover and allow for viral expression. Mice were habituated to restraint for attaching optical fibers for 3 days immediately prior to instrumental conditioning. During instrumental conditioning, mice were tethered to a 100-µm diameter optic fiber bifurcated patchcord (Inper) attached to a 593-nm laser (Dragon Laser) via a rotary joint. Mice were habituated to the tether during the magazine training session, but no laser was delivered. Beginning with the first FR-1 session, all subjects received laser delivery during reward collection (first magazine entry after reward delivery; 5-s pulse, 8-10 mW). After completion of FR-1, mice received 1 session each of instrumental conditioning on an RR-2, RR-5, and RR-10 reinforcement schedule (max 20 outcomes/20 min/session). We chose an RR schedule of reinforcement for this experiment because tends to promote action-outcome learning and goal-directed behavioral control [94,95,100,123] and, thus, would make it more difficult to neurobiologically induce habit formation, increasing the robustness of the results. Following training mice received a counterbalanced set of sensory-specific satiety outcome-specific devaluation tests, as above. Mice were tethered but no laser was delivered on test days. Mice received laser as in training during the intervening retraining session. After instrumental training and testing, mice were tested in the RTPP test as described above. Mice were then perfused and brain tissue was processed with standard histology procedures described below to assess viral expression location/spread and fiber placement.

Chemogenetic inactivation of CeA→DMS projections during instrumental learning following CUS

Male and female (mCherry *N* = 32, 16 male; hM4Di: *N* = 32, 16 male) naïve mice were used in this experiment to assess the necessity of CeA→DMS projection activity during learning for stress-potentiated habit formation. 16 subjects with off-target viral expression and 3 subjects that did not complete instrumental conditioning were excluded from the dataset. Mice were randomly assigned to Viral and Stress groups. At surgery, all mice received bilateral infusion of the retrogradely-trafficked CAV encoding cre-recombinase (CAV2-Cre-GFP; Plateforme de Vectorologie de Montpellier) into the DMS (0.3 µl) and AAV encoding the cre-inducible inhibitory designer receptor human M4 muscarinic receptor (hM4DGi; AAV2-Syn-DIO-hM4Di-mCherry; Addgene) or fluorophore control (AAV2-Syn-DIO-mCherry; Addgene) into the CeA (0.1-0.2 µl). Mice were given 1-2 weeks to recover post-surgery, followed by 14 consecutive days of twice/daily CUS or daily handling as described above. Mice were habituated to i.p. injections during the final 3 days of the CUS/handling period. 24 hours after the final CUS

exposure, mice began instrumental conditioning as described above. All subjects received an intraperitoneal (i.p.) injection of CNO (2 mg/kg[106,107,164,165]; Hello Bio) 30 min prior to each instrumental conditioning session. Upon completion of FR-1, mice received 1 session of training on an RI-15s reinforcement schedule followed by 2 sessions on the RI-30s schedule (max 30 outcomes/30 min/session). We chose an RI reinforcement schedule for this experiment because it tends to promote habit formation [94,95,100,123] and, thus, would make it more difficult to neurobiologically prevent stress-potentiated habit, increasing the robustness of the results. Following training, mice received a counterbalanced pair of sensory-specific satiety outcome-specific devaluation tests, as above. No CNO was given on test days. CNO was given prior to the retraining session. After instrumental training and testing, mice were then perfused and brain tissue was processed with standard histology procedures described below to assess viral expression location and spread.

Optogenetic inactivation of CeA→DMS projections during instrumental learning following CUS

Male and female (control, GFP *N* = 18, 11 male; control, Arch: *N* = 26, 12 male) naïve mice were used in this experiment to assess the necessity of CeA→DMS projection activity at outcome experience during learning for stress-potentiated habit formation. 10 subjects with off-target viral expression or fiber location and 2 subjects that did not complete instrumental conditioning were excluded from the dataset. Mice were randomly assigned to Virus and Stress groups. At surgery, mice received bilateral infusion an AAV encoding the inhibitory opsin Arch (AAVDJ-Syn-eArch-eYFP, Stanford Vector Core) or fluorophore control (AAV8-Syn-GFP; Addgene) into the CeA (0.1-0.2 µl). Optic fiber cannulae (2.4-mm length, 100-µm diameter, 0.22 NA, Inper) were implanted over the DMS. Mice were given 1 - 2 weeks to recover post-surgery, followed by 14 consecutive days of twice/daily CUS or daily handling as described above. Mice were habituated to restraint for attaching optical fibers during the final 3 days of the CUS/handling period. 24 hours after the final CUS exposure, mice began instrumental conditioning as described above. During instrumental conditioning, mice were tethered to a 100-µm diameter optic fiber bifurcated patchcord (Inper) attached to a 593-nm laser (Dragon Laser) via a rotary joint. Mice were habituated to the tether during the magazine training session, but no laser was delivered. Beginning with the first FR-1 session, all subjects received laser delivery during reward collection, (first magazine entry after reward delivery; 5-s pulse, 8-10 mW). After completion of FR-1, mice received 1 training session on an RI-15s reinforcement schedule and 2 training sessions on the RI-30s schedule (max 20 outcomes/20 min/session). We chose an RI reinforcement schedule for this experiment because it tends to promote habit formation [94,95,100,123] and, thus, would make it more difficult to neurobiologically prevent stress-potentiated habit, increasing the robustness of the results. Following training, mice received a counterbalanced set of sensory-specific satiety outcome-specific devaluation tests, as above. Mice were tethered but no laser was delivered on test days. Mice received laser as in training during the intervening retraining session. After instrumental training and testing, mice were tested in the RTPP test as described above. Mice were then perfused and brain tissue was processed with standard histology procedures described below to assess viral expression location/spread and fiber placement.

Optogenetic activation of CeA→DMS projections during instrumental learning

Male and female (GFP *N* = 18, 9 male; ChR2: *N* = 20, 12 male) naïve mice were used in this experiment to assess whether CeA→DMS projection activation at outcome experience during learning is sufficient to promote habit formation. 11 subjects with off-target viral expression or fiber location and 4 subjects who did not complete instrumental conditioning were excluded from the dataset. Mice were randomly assigned to Virus group. Given the low density of CeA→DMS projections, we choose to activate DMS-projecting CeA cell bodies. At surgery, mice received bilateral infusion of a retrogradely trafficked AAV encoding cre-recombinase (AAVrg-Syn-Cre-P2A-dTomato, Addgene) into the DMS (0.3 µl) and AAV encoding the cre-inducible excitatory opsin channelrhodopsin 2 (ChR2; AAV8-Syn-DIO-ChR2-eYFP, Stanford Vector Core) or fluorophore control (AAV8-Syn-DIO-eYFP, Stanford Vector Core) into the CeA (0.1-0.2 µl). Optic fiber cannulae (4.4-mm length, 100-µm diameter, 0.22 NA, Inper) were implanted over the CeA. Mice were given 3 weeks to recover and allow for viral expression. Mice were habituated to restraint for 3 days prior to instrumental conditioning. During instrumental conditioning, mice were tethered to a 100-µm diameter optic fiber bifurcated patchcord (Inper) attached to a 473-nm laser (Dragon Laser) via a rotary joint. Mice were habituated to the tether during the magazine training session, but no laser was delivered. Beginning with the first FR-1 session, all subjects received laser delivery during reward collection (first magazine entry after reward delivery; 2-s duration, 20 Hz, 5-ms pulse width, 8-10 mW). After completion of FR-1, mice received 1 day each of training on an RR-2, RR-5, and RR-10 reinforcement schedule (max 20 outcomes/20 min/session). We chose an RR schedule of reinforcement for this experiment

because it tends to promote action-outcome learning and goal-directed behavioral control [94,95,100,123] and, thus, would make it more difficult to neurobiologically induce habit formation, increasing the robustness of the results. Following training mice received a counterbalanced set of sensory-specific satiety outcome-specific devaluation tests, as above. Mice were tethered but no laser was delivered on test days. Mice received laser as in training during the intervening retraining session. After instrumental training and testing, mice were tested in the RTPP test, as described above. Mice were then perfused and brain tissue was processed with standard histology procedures described below to assess viral expression location/spread and fiber placement.

Optogenetic activation of CeA→DMS projections during instrumental learning following sub-threshold CUS

Male and female (GFP *N* = 12, 5 male; ChR2: *N* = 18, 8 male) naïve mice were used in this experiment to assess whether CeA→DMS projection activation at outcome experience during learning is sufficient to promote habit formation in mice with a history of less-frequent CUS (subthreshold for promoting habit formation). 9 subjects with off-target viral expression or fiber location and 3 subjects who did not complete instrumental conditioning were excluded from the dataset. Mice were randomly assigned to viral groups. Similar to optogenetic activation of CeA→DMS neurons in control mice, we chose to target cell bodies with this approach. At surgery, mice received bilateral infusion of a retrogradely trafficked AAV encoding cre-recombinase (AAVrg-Syn-Cre-P2A-dTomato, Addgene) into the DMS (0.3 µl) and AAV encoding the cre-inducible excitatory opsin ChR2 (AAV8-Syn-DIO-ChR2-eYFP, Stanford Vector Core) or fluorophore control (AAV8-Syn-DIO-eYFP, Stanford Vector Core) into the CeA (0.1-0.2 µl). Optic fiber cannulae (4.4-mm length, 100-µm diameter, 0.22 NA, Inper) were implanted over the CeA. Mice were given 1 - 2 weeks to recover post-surgery, followed by 14 consecutive days of once/daily CUS or daily handling as described above. Mice were habituated to restraint for attaching optical fibers during the final 3 days of the subthreshold CUS/handling period. 24 hours after the final stress exposure, mice began instrumental conditioning, as described above. During instrumental conditioning, mice were tethered to a 100-µm diameter optic fiber bifurcated patchcord (Inper) attached to a 473-nm laser (Dragon Laser) via a rotary joint. Mice were habituated to the tether during the magazine training session, but no laser was delivered. Beginning with the first FR-1 session, all subjects received laser delivery during reward collection, (first magazine entry after reward delivery; 2-s duration, 20 Hz, 5-ms pulse width, 8-10 mW). After completion of FR-1, mice received 1 day each of training on an RR-2, RR-5, and RR-10 reinforcement schedule (max 20 outcomes/20 min/session). Following training mice received a counterbalanced set of sensory-specific satiety outcome-specific devaluation tests, as above. Mice were tethered but no laser was delivered on test days. Mice received laser during the intervening retraining session. After instrumental training and testing, mice were tested in the RTPP test, as described above. Mice were then perfused and brain tissue was processed with standard histology procedures described below to assess viral expression location/spread and fiber placement.

Immunohistochemistry

Mice were anesthetized with isoflurane and transcardially perfused with ice-cold PBS followed by cold 4% paraformaldehyde. The brains were removed, post-fixed in 4% paraformaldehyde, then cryoprotected in 30% sucrose in PBS. 30-µm coronal slices were taken on a cryostat and collected in PBS. Immunohistochemical analysis was performed as described previously[162,166-168]. Briefly, floating sections were blocked for 1 hour at room temperature in blocking solution (3% normal goat serum (NGS, Jackson ImmunoResearch Laboratories), 0.3% Triton X-100 (Fisher)) in PBS and then incubated overnight with gentle agitation at 4 °C in blocking solution plus 1:1000 dilution primary antibody (chicken anti-GFP polyclonal, Abcam; rabbit anti-dsRed polyclonal, Takara Bio). Sections were then incubated covered with gentle agitation for 2 hours at room temperature in blocking solution plus 1:500 dilution secondary antibody (goat anti-rabbit IgG Alexafluor 594 conjugate; goat anti-chicken IgG Alexafluor 488 conjugate, Invitrogen). All sections were washed 3 times for 5 min each in PBS before and after each incubation step and mounted on slides using ProLong Gold antifade reagent with DAPI (Invitrogen). All images were acquired using a Keyence (BZ-X710) microscope with 4X, 10X, and 20X objectives (CFI Plan Apo), CCD camera, and BZ-X Analyze software and a Zeiss Confocal LSM with 2.5X and 20X objectives and Zeiss ZEN (blue edition) image acquisition software.

Statistical Analysis

Datasets were analyzed by 2-tailed t-tests, or 1-, 2-, or 3-way repeated-measures analysis of variance (ANOVA), as appropriate (GraphPad Prism, GraphPad, San Diego, CA; SPSS, IBM, Chicago, IL). Some datasets were slightly non-normally distributed. For these datasets statistical tests were also run on the normally-distributed

log-transformed data and the results were highly consistent (Supplemental Table 4). We opted to use parametric statistics for consistency across experiments and given evidence that ANOVA is robust to slight non-normality[169,170]. Bonferroni post hoc tests corrected for multiple comparisons were performed to clarify statistical interactions. Greenhouse-Geisser correction was applied to mitigate the influence of unequal variance between conditions. Alpha levels were set at $P < 0.05$.

Sex as a biological variable

For the initial behavioral finding, sex was included as a factor in the ANOVA and found to not significantly account for variance (No main effect of Sex on lever pressing acquisition: $F_{(1, 43)} = 0.43$, $P = 0.51$, devaluation test press rate: $F_{(1,43)} = 0.60$, $P = 0.44$, or devaluation index: $F_{(1,43)} = 0.04$, $P = 0.84$). Therefore, data from male and female mice was combined for analyses. For subsequent experiments, male and female mice were used in approximately equal numbers, but the N per sex was underpowered to examine sex differences. Sex was therefore not included as a factor in statistical analyses, though individual data points are visually disaggregated by sex.

Rigor and reproducibility

Group sizes were estimated based on prior work with this behavioral task[171] and to ensure counterbalancing of virus, stress, pellet type, and devaluation test order. Investigators were not blinded to viral or stress group because they were required to administer infusions and stress exposure. All behaviors were scored using automated software (Med Associates). Each experiment included at least 1 replication cohort and cohorts were balanced by Viral group, Stress group, and hemisphere (for photometry recordings and tracing) prior to the start of the experiment. Investigators were blinded to group when performing histological validation and determining exclusions based on viral spread or mistargeted implant.

Data and code availability

All data that support the findings of this study are available from the corresponding author upon request. Custom-written MATLAB code is accessible via Dryad repository[172] and available from the corresponding author upon request.

REFERENCES

1 Wassum, K. M. Amygdala-cortical collaboration in reward learning and decision making. *Elife* **11** (2022). https://doi.org/10.7554/eLife.80926

2 Balleine, B. W. The Meaning of Behavior: Discriminating Reflex and Volition in the Brain. *Neuron* **104**, 47-62 (2019). https://doi.org/10.1016/j.neuron.2019.09.024

3 Balleine, B. W. & Dickinson, A. Goal-directed instrumental action: contingency and incentive learning and their cortical substrates. *Neuropharmacology* **37**, 407-419 (1998).

4 Malvaez, M. & Wassum, K. Regulation of habit formation in the dorsal striatum. *Current Opinion in Behavioral Sciences* **20**, 67-74 (2018).

5 Graybiel, A. M. Habits, rituals, and the evaluative brain. *Annu Rev Neurosci* **31**, 359-387 (2008). https://doi.org/10.1146/annurev.neuro.29.051605.112851

6 Adams, C. D. Variations in the sensitivity of instrumental responding to reinforcer devaluation. *Quarterly Journal of Experimental Psychology* **34**, 77-98 (1982).

7 Smith, K. S. & Graybiel, A. M. Habit formation. *Dialogues Clin Neurosci* **18**, 33-43 (2016).

8 Dickinson, A. Actions and Habits: the development of behavioural autonomy. *Philosphical Transactions of the Royal Society of London* **B308**, 67-78 (1985).

9 Dolan, R. J. & Dayan, P. Goals and habits in the brain. *Neuron* **80**, 312-325 (2013). https://doi.org/10.1016/j.neuron.2013.09.007

10 Redish, A. D., Jensen, S. & Johnson, A. A unified framework for addiction: vulnerabilities in the decision process. *Behav Brain Sci* **31**, 415-437; discussion 437-487 (2008). https://doi.org/10.1017/S0140525X0800472X

11 Vandaele, Y. & Ahmed, S. H. Habit, choice, and addiction. *Neuropsychopharmacology* **46**, 689-698 (2021). https://doi.org/10.1038/s41386-020-00899-y

12 Voon, V. *et al.* Disorders of compulsivity: a common bias towards learning habits. *Mol Psychiatry* **20**, 345-352 (2015). https://doi.org/10.1038/mp.2014.44

13 Gillan, C. M., Robbins, T. W., Sahakian, B. J., van den Heuvel, O. A. & van Wingen, G. The role of habit in compulsivity. *Eur Neuropsychopharmacol* **26**, 828-840 (2016). https://doi.org/10.1016/j.euroneuro.2015.12.033

14 Corbit, L. H. & Janak, P. H. Habitual Alcohol Seeking: Neural Bases and Possible Relations to Alcohol Use Disorders. *Alcohol Clin Exp Res* (2016). https://doi.org/10.1111/acer.13094

15 Ostlund, S. B. & Balleine, B. W. On habits and addiction: An associative analysis of compulsive drug seeking. *Drug Discov Today Dis Models* **5**, 235-245 (2008). https://doi.org/10.1016/j.ddmod.2009.07.004

16 Zapata, A., Minney, V. L. & Shippenberg, T. S. Shift from goal-directed to habitual cocaine seeking after prolonged experience in rats. *J Neurosci* **30**, 15457-15463 (2010). https://doi.org/10.1523/JNEUROSCI.4072-10.2010

17 Hogarth, L. & Chase, H. W. Parallel goal-directed and habitual control of human drug-seeking: Implications for dependence vulnerability. *J Exp Psychol Anim Behav Process* (2011).

18 Belin, D., Belin-Rauscent, A., Murray, J. E. & Everitt, B. J. Addiction: failure of control over maladaptive incentive habits. *Curr Opin Neurobiol* (2013). https://doi.org/10.1016/j.conb.2013.01.025

19 Hogarth, L., Balleine, B. W., Corbit, L. H. & Killcross, S. Associative learning mechanisms underpinning the transition from recreational drug use to addiction. *Ann N Y Acad Sci* **1282**, 12-24 (2013). https://doi.org/10.1111/j.1749-6632.2012.06768.x

20 Leblanc, K. H., Maidment, N. T. & Ostlund, S. B. Repeated cocaine exposure facilitates the expression of incentive motivation and induces habitual control in rats. *PLoS One* **8**, e61355 (2013). https://doi.org/10.1371/journal.pone.0061355

21 Furlong, T. M., Jayaweera, H. K., Balleine, B. W. & Corbit, L. H. Binge-like consumption of a palatable food accelerates habitual control of behavior and is dependent on activation of the dorsolateral striatum. *J Neurosci* **34**, 5012-5022 (2014). https://doi.org/10.1523/JNEUROSCI.3707-13.2014

22 Renteria, R., Baltz, E. T. & Gremel, C. M. Chronic alcohol exposure disrupts top-down control over basal ganglia action selection to produce habits. *Nat Commun* **9**, 211 (2018). https://doi.org/10.1038/s41467-017-02615-9

23 Hogarth, L., Attwood, A. S., Bate, H. A. & Munafò, M. R. Acute alcohol impairs human goal-directed action. *Biol Psychol* **90**, 154-160 (2012). https://doi.org/10.1016/j.biopsycho.2012.02.016

24 Ray, L. A. *et al.* Capturing habitualness of drinking and smoking behavior in humans. *Drug Alcohol Depend* **207**, 107738 (2020). https://doi.org/10.1016/j.drugalcdep.2019.107738

25 Groman, S. M., Massi, B., Mathias, S. R., Lee, D. & Taylor, J. R. Model-Free and Model-Based Influences in Addiction-Related Behaviors. *Biol Psychiatry* **85**, 936-945 (2019). https://doi.org/10.1016/j.biopsych.2018.12.017

26 Gillan, C. M. *et al.* Disruption in the balance between goal-directed behavior and habit learning in obsessive-compulsive disorder. *Am J Psychiatry* **168**, 718-726 (2011). https://doi.org/10.1176/appi.ajp.2011.10071062

27 Gillan, C. M. *et al.* Enhanced avoidance habits in obsessive-compulsive disorder. *Biol Psychiatry* **75**, 631-638 (2014). https://doi.org/10.1016/j.biopsych.2013.02.002

28 Vaghi, M. M. *et al.* Action-Outcome Knowledge Dissociates From Behavior in Obsessive-Compulsive Disorder Following Contingency Degradation. *Biol Psychiatry Cogn Neurosci Neuroimaging* **4**, 200-209 (2019). https://doi.org/10.1016/j.bpsc.2018.09.014

29 Horstmann, A. *et al.* Slave to habit? Obesity is associated with decreased behavioural sensitivity to reward devaluation. *Appetite* **87**, 175-183 (2015). https://doi.org/10.1016/j.appet.2014.12.212

30 Morris, R. W., Cyrzon, C., Green, M. J., Le Pelley, M. E. & Balleine, B. W. Impairments in action-outcome learning in schizophrenia. *Transl Psychiatry* **8**, 54 (2018). https://doi.org/10.1038/s41398-018-0103-0

31 Griffiths, K. R., Morris, R. W. & Balleine, B. W. Translational studies of goal-directed action as a framework for classifying deficits across psychiatric disorders. *Front Syst Neurosci* **8**, 101 (2014). https://doi.org/10.3389/fnsys.2014.00101

32 Morris, R. W., Quail, S., Griffiths, K. R., Green, M. J. & Balleine, B. W. Corticostriatal control of goal-directed action is impaired in schizophrenia. *Biol Psychiatry* **77**, 187-195 (2015). https://doi.org/10.1016/j.biopsych.2014.06.005

33 Byrne, K. A., Six, S. G. & Willis, H. C. Examining the effect of depressive symptoms on habit formation and habit-breaking. *J Behav Ther Exp Psychiatry* **73**, 101676 (2021). https://doi.org/10.1016/j.jbtep.2021.101676

34 Alvares, G. A., Balleine, B. W. & Guastella, A. J. Impairments in goal-directed actions predict treatment response to cognitive-behavioral therapy in social anxiety disorder. *PLoS One* **9**, e94778 (2014). https://doi.org/10.1371/journal.pone.0094778

35 Alvares, G. A., Balleine, B. W., Whittle, L. & Guastella, A. J. Reduced goal-directed action control in autism spectrum disorder. *Autism Res* (2016). https://doi.org/10.1002/aur.1613

36 Soares, J. M. *et al.* Stress-induced changes in human decision-making are reversible. *Transl Psychiatry* **2**, e131 (2012). https://doi.org/10.1038/tp.2012.59

37 Schwabe, L. & Wolf, O. T. Stress-induced modulation of instrumental behavior: from goal-directed to habitual control of action. *Behav Brain Res* **219**, 321-328 (2011). https://doi.org/10.1016/j.bbr.2010.12.038

38 Schwabe, L. & Wolf, O. T. Stress prompts habit behavior in humans. *J Neurosci* **29**, 7191-7198 (2009).

39 Schwabe, L., Dickinson, A. & Wolf, O. T. Stress, habits, and drug addiction: a psychoneuroendocrinological perspective. *Exp Clin Psychopharmacol* **19**, 53-63 (2011). https://doi.org/10.1037/a0022212

40 Fournier, M., d'Arripe-Longueville, F. & Radel, R. Effects of psychosocial stress on the goal-directed and habit memory systems during learning and later execution. *Psychoneuroendocrinology* **77**, 275-283 (2017). https://doi.org/10.1016/j.psyneuen.2016.12.008

41 Pool, E. R. *et al.* Determining the effects of training duration on the behavioral expression of habitual control in humans: a multilaboratory investigation. *Learn Mem* **29**, 16-28 (2022). https://doi.org/10.1101/lm.053413.121

42 Friedel, E. *et al.* How Accumulated Real Life Stress Experience and Cognitive Speed Interact on Decision-Making Processes. *Front Hum Neurosci* **11**, 302 (2017). https://doi.org/10.3389/fnhum.2017.00302

43 Meier, J. K., Staresina, B. P. & Schwabe, L. Stress diminishes outcome but enhances response representations during instrumental learning. *Elife* **11** (2022). https://doi.org/10.7554/eLife.67517

44 Quaedflieg, C. W. E. M., Stoffregen, H., Sebalo, I. & Smeets, T. Stress-induced impairment in goal-directed instrumental behaviour is moderated by baseline working memory. *Neurobiol Learn Mem* **158**, 42-49 (2019). https://doi.org/10.1016/j.nlm.2019.01.010

45 Kalia, V. & Knauft, K. Emotion regulation strategies modulate the effect of adverse childhood experiences on perceived chronic stress with implications for cognitive flexibility. *PLoS One* **15**, e0235412 (2020). https://doi.org/10.1371/journal.pone.0235412

46 Gordon, A. L., Patterson, T. K. & Knowlton, B. J. Early-life stress is associated with a preponderance of habitual responding in a novel instrumental avoidance learning paradigm. *Neurobiol Learn Mem* **175**, 107316 (2020). https://doi.org/10.1016/j.nlm.2020.107316

47 Patterson, T. K., Craske, M. G. & Knowlton, B. J. Enhanced Avoidance Habits in Relation to History of Early-Life Stress. *Front Psychol* **10**, 1876 (2019). https://doi.org/10.3389/fpsyg.2019.01876

48 Leong, K. C. & Packard, M. G. Exposure to predator odor influences the relative use of multiple memory systems: role of basolateral amygdala. *Neurobiol Learn Mem* **109**, 56-61 (2014). https://doi.org/10.1016/j.nlm.2013.11.015

49 Schwabe, L., Dalm, S., Schächinger, H. & Oitzl, M. S. Chronic stress modulates the use of spatial and stimulus-response learning strategies in mice and man. *Neurobiol Learn Mem* **90**, 495-503 (2008). https://doi.org/10.1016/j.nlm.2008.07.015

50 Sadowski, R. N., Jackson, G. R., Wieczorek, L. & Gold, P. E. Effects of stress, corticosterone, and epinephrine administration on learning in place and response tasks. *Behav Brain Res* **205**, 19-25 (2009). https://doi.org/10.1016/j.bbr.2009.06.027

51 Grissom, E. M. *et al.* Learning strategy is influenced by trait anxiety and early rearing conditions in prepubertal male, but not prepubertal female rats. *Neurobiol Learn Mem* **98**, 174-181 (2012). https://doi.org/10.1016/j.nlm.2012.06.001

52 Goodman, J. & McIntyre, C. K. Impaired Spatial Memory and Enhanced Habit Memory in a Rat Model of Post-traumatic Stress Disorder. *Front Pharmacol* **8**, 663 (2017). https://doi.org/10.3389/fphar.2017.00663

53 Lormant, F. *et al.* Training level reveals a dynamic dialogue between stress and memory systems in birds. *Behav Brain Res* **408**, 113280 (2021). https://doi.org/10.1016/j.bbr.2021.113280

54 Packard, M. G. & Gabriele, A. Peripheral anxiogenic drug injections differentially affect cognitive and habit memory: role of basolateral amygdala. *Neuroscience* **164**, 457-462 (2009). https://doi.org/10.1016/j.neuroscience.2009.07.054

55 Packard, M. G. & Wingard, J. C. Amygdala and "emotional" modulation of the relative use of multiple memory systems. *Neurobiol Learn Mem* **82**, 243-252 (2004). https://doi.org/10.1016/j.nlm.2004.06.008

56 Gourley, S. L. *et al.* Action control is mediated by prefrontal BDNF and glucocorticoid receptor binding. *Proc Natl Acad Sci U S A* **109**, 20714-20719 (2012). https://doi.org/10.1073/pnas.1208342109

57 Dieterich, A. *et al.* Chronic corticosterone administration induces negative valence and impairs positive valence behaviors in mice. *Transl Psychiatry* **9**, 337 (2019). https://doi.org/10.1038/s41398-019-0674-4

58 Alizamini, M. M. *et al.* Corticotropin-releasing factor receptor 1 in infralimbic cortex modulates social stress-altered decision-making. *Prog Neuropsychopharmacol Biol Psychiatry* **116**, 110523 (2022). https://doi.org/10.1016/j.pnpbp.2022.110523

59 Hinton, E. A., Li, D. C., Allen, A. G. & Gourley, S. L. Social Isolation in Adolescence Disrupts Cortical Development and Goal-Dependent Decision-Making in Adulthood, Despite Social Reintegration. *eNeuro* **6** (2019). https://doi.org/10.1523/ENEURO.0318-19.2019

60 Dias-Ferreira, E. *et al.* Chronic stress causes frontostriatal reorganization and affects decision-making. *Science* **325**, 621-625 (2009). https://doi.org/10.1126/science.1171203

61 Koob, G. F. Alcoholism: allostasis and beyond. *Alcohol Clin Exp Res* **27**, 232-243 (2003).

62 Agid, O., Kohn, Y. & Lerer, B. Environmental stress and psychiatric illness. *Biomed Pharmacother* **54**, 135-141 (2000). https://doi.org/10.1016/S0753-3322(00)89046-0

63 Baumeister, D., Lightman, S. L. & Pariante, C. M. The Interface of Stress and the HPA Axis in Behavioural Phenotypes of Mental Illness. *Curr Top Behav Neurosci* **18**, 13-24 (2014). https://doi.org/10.1007/7854_2014_304

64 María-Ríos, C. E. & Morrow, J. D. Mechanisms of Shared Vulnerability to Post-traumatic Stress Disorder and Substance Use Disorders. *Front Behav Neurosci* **14**, 6 (2020). https://doi.org/10.3389/fnbeh.2020.00006

65 Brady, K. T. & Sinha, R. Co-occurring mental and substance use disorders: the neurobiological effects of chronic stress. *Am J Psychiatry* **162**, 1483-1493 (2005). https://doi.org/10.1176/appi.ajp.162.8.1483

66 Duffing, T. M., Greiner, S. G., Mathias, C. W. & Dougherty, D. M. Stress, substance abuse, and addiction. *Curr Top Behav Neurosci* **18**, 237-263 (2014). https://doi.org/10.1007/7854_2014_276
67 Malvaez, M. Neural substrates of habit. *J Neurosci Res* (2019). https://doi.org/10.1002/jnr.24552
68 Balleine, B. W. & O'Doherty, J. P. Human and rodent homologies in action control: corticostriatal determinants of goal-directed and habitual action. *Neuropsychopharmacology* **35**, 48-69 (2010). https://doi.org/10.1038/npp.2009.131
69 Balleine, B. W., Delgado, M. R. & Hikosaka, O. The role of the dorsal striatum in reward and decision-making. *J Neurosci* **27**, 8161-8165 (2007). https://doi.org/10.1523/JNEUROSCI.1554-07.2007
70 Yin, H. H., Knowlton, B. J. & Balleine, B. W. Blockade of NMDA receptors in the dorsomedial striatum prevents action-outcome learning in instrumental conditioning. *Eur J Neurosci* **22**, 505-512 (2005).
71 Corbit, L. H. & Janak, P. H. Posterior dorsomedial striatum is critical for both selective instrumental and Pavlovian reward learning. *Eur J Neurosci* **31**, 1312-1321 (2010). https://doi.org/10.1111/j.1460-9568.2010.07153.x
72 Lex, B. & Hauber, W. The role of dopamine in the prelimbic cortex and the dorsomedial striatum in instrumental conditioning. *Cereb Cortex* **20**, 873-883 (2010). https://doi.org/10.1093/cercor/bhp151
73 Liljeholm, M., Tricomi, E., O'Doherty, J. P. & Balleine, B. W. Neural correlates of instrumental contingency learning: differential effects of action-reward conjunction and disjunction. *J Neurosci* **31**, 2474-2480 (2011). https://doi.org/10.1523/JNEUROSCI.3354-10.2011
74 McNamee, D., Liljeholm, M., Zika, O. & O'Doherty, J. P. Characterizing the associative content of brain structures involved in habitual and goal-directed actions in humans: a multivariate FMRI study. *J Neurosci* **35**, 3764-3771 (2015). https://doi.org/10.1523/JNEUROSCI.4677-14.2015
75 O'Hare, J., Calakos, N. & Yin, H. H. Recent Insights into Corticostriatal Circuit Mechanisms underlying Habits: Invited review for Current Opinions in Behavioral Sciences. *Curr Opin Behav Sci* **20**, 40-46 (2018). https://doi.org/10.1016/j.cobeha.2017.10.001
76 Yin, H. H., Ostlund, S. B., Knowlton, B. J. & Balleine, B. W. The role of the dorsomedial striatum in instrumental conditioning. *Eur J Neurosci* **22**, 513-523 (2005).
77 Balleine, B. W., Killcross, A. S. & Dickinson, A. The effect of lesions of the basolateral amygdala on instrumental conditioning. *J Neurosci* **23**, 666-675 (2003).
78 Ostlund, S. B. & Balleine, B. W. Differential involvement of the basolateral amygdala and mediodorsal thalamus in instrumental action selection. *J Neurosci* **28**, 4398-4405 (2008).
79 Lingawi, N. W. & Balleine, B. W. Amygdala central nucleus interacts with dorsolateral striatum to regulate the acquisition of habits. *J Neurosci* **32**, 1073-1081 (2012). https://doi.org/10.1523/JNEUROSCI.4806-11.2012
80 Pan, W. X., Mao, T. & Dudman, J. T. Inputs to the dorsal striatum of the mouse reflect the parallel circuit architecture of the forebrain. *Front Neuroanat* **4**, 147 (2010). https://doi.org/10.3389/fnana.2010.00147
81 Wall, N. R., De La Parra, M., Callaway, E. M. & Kreitzer, A. C. Differential innervation of direct- and indirect-pathway striatal projection neurons. *Neuron* **79**, 347-360 (2013). https://doi.org/10.1016/j.neuron.2013.05.014
82 Corbit, L. H., Leung, B. K. & Balleine, B. W. The role of the amygdala-striatal pathway in the acquisition and performance of goal-directed instrumental actions. *J Neurosci* **33**, 17682-17690 (2013). https://doi.org/10.1523/JNEUROSCI.3271-13.2013
83 Kelley, A. E., Domesick, V. B. & Nauta, W. J. The amygdalostriatal projection in the rat--an anatomical study by anterograde and retrograde tracing methods. *Neuroscience* **7**, 615-630 (1982).
84 Kita, H. & Kitai, S. T. Amygdaloid projections to the frontal cortex and the striatum in the rat. *J Comp Neurol* **298**, 40-49 (1990). https://doi.org/10.1002/cne.902980104
85 McDonald, A. J. Topographical organization of amygdaloid projections to the caudatoputamen, nucleus accumbens, and related striatal-like areas of the rat brain. *Neuroscience* **44**, 15-33 (1991).
86 McDonald, A. J. Organization of amygdaloid projections to the prefrontal cortex and associated striatum in the rat. *Neuroscience* **44**, 1-14 (1991).
87 Swanson, L. W. & Petrovich, G. D. What is the amygdala? *Trends Neurosci* **21**, 323-331 (1998).
88 Ehrlich, I. *et al.* Amygdala inhibitory circuits and the control of fear memory. *Neuron* **62**, 757-771 (2009). https://doi.org/10.1016/j.neuron.2009.05.026
89 Gilpin, N. W., Herman, M. A. & Roberto, M. The central amygdala as an integrative hub for anxiety and alcohol use disorders. *Biol Psychiatry* **77**, 859-869 (2015). https://doi.org/10.1016/j.biopsych.2014.09.008
90 Moscarello, J. M. & Penzo, M. A. The central nucleus of the amygdala and the construction of defensive modes across the threat-imminence continuum. *Nat Neurosci* **25**, 999-1008 (2022). https://doi.org/10.1038/s41593-022-01130-5
91 Roozendaal, B., McEwen, B. S. & Chattarji, S. Stress, memory and the amygdala. *Nat Rev Neurosci* **10**, 423-433 (2009). https://doi.org/10.1038/nrn2651
92 Zhang, W. H., Zhang, J. Y., Holmes, A. & Pan, B. X. Amygdala Circuit Substrates for Stress Adaptation and Adversity. *Biol Psychiatry* **89**, 847-856 (2021). https://doi.org/10.1016/j.biopsych.2020.12.026
93 Wassum, K. M., Cely, I. C., Maidment, N. T. & Balleine, B. W. Disruption of endogenous opioid activity during instrumental learning enhances habit acquisition. *Neuroscience* **163**, 770-780 (2009).
94 Hilário, M. R., Clouse, E., Yin, H. H. & Costa, R. M. Endocannabinoid signaling is critical for habit formation. *Front Integr Neurosci* **1**, 6 (2007). https://doi.org/10.3389/neuro.07.006.2007
95 Dickinson, A. D., Nicholas, J. & Adams, C. D. The effect of the instrumental training contingency on susceptibility to reinforcer devaluation. *Quarterly Journal of Experimental Psychology* **35.1**, 35-51 (1983).
96 Garr, E., Padovan-Hernandez, Y., Janak, P. H. & Delamater, A. R. Maintained goal-directed control with overtraining on ratio schedules. *Learn Mem* **28**, 435-439 (2021). https://doi.org/10.1101/lm.053472.121
97 Malvaez, M. *et al.* Habits Are Negatively Regulated by Histone Deacetylase 3 in the Dorsal Striatum. *Biol Psychiatry* (2018). https://doi.org/10.1016/j.biopsych.2018.01.025
98 Dickinson, A. & Balleine, B. W. (1994).

99 Robbins, T. W. & Costa, R. M. Habits. *Curr Biol* **27**, R1200-R1206 (2017). https://doi.org/10.1016/j.cub.2017.09.060

100 Adams, C. D. & Dickinson, A. Instrumental responding following reinforcer devaluation. *The Quarterly Journal of Experimental Psychology* **33**, 109-121 (1981).

101 Alexander, G. M. *et al.* Remote control of neuronal activity in transgenic mice expressing evolved G protein-coupled receptors. *Neuron* **63**, 27-39 (2009). https://doi.org/10.1016/j.neuron.2009.06.014

102 Vazey, E. M. & Aston-Jones, G. Designer receptor manipulations reveal a role of the locus coeruleus noradrenergic system in isoflurane general anesthesia. *Proc Natl Acad Sci U S A* **111**, 3859-3864 (2014). https://doi.org/10.1073/pnas.1310025111

103 Qiu, M. H., Chen, M. C., Fuller, P. M. & Lu, J. Stimulation of the Pontine Parabrachial Nucleus Promotes Wakefulness via Extra-thalamic Forebrain Circuit Nodes. *Curr Biol* **26**, 2301-2312 (2016). https://doi.org/10.1016/j.cub.2016.07.054

104 Zhu, H. *et al.* Cre-dependent DREADD (Designer Receptors Exclusively Activated by Designer Drugs) mice. *Genesis* **54**, 439-446 (2016). https://doi.org/10.1002/dvg.22949

105 Pomrenze, M. B. *et al.* A Transgenic Rat for Investigating the Anatomy and Function of Corticotrophin Releasing Factor Circuits. *Front Neurosci* **9**, 487 (2015). https://doi.org/10.3389/fnins.2015.00487

106 Tipps, M., Marron Fernandez de Velasco, E., Schaeffer, A. & Wickman, K. Inhibition of Pyramidal Neurons in the Basal Amygdala Promotes Fear Learning. *eNeuro* **5** (2018). https://doi.org/10.1523/ENEURO.0272-18.2018

107 Tuscher, J. J., Taxier, L. R., Fortress, A. M. & Frick, K. M. Chemogenetic inactivation of the dorsal hippocampus and medial prefrontal cortex, individually and concurrently, impairs object recognition and spatial memory consolidation in female mice. *Neurobiol Learn Mem* **156**, 103-116 (2018). https://doi.org/10.1016/j.nlm.2018.11.002

108 Fisher, S. D., Ferguson, L. A., Bertran-Gonzalez, J. & Balleine, B. W. Amygdala-Cortical Control of Striatal Plasticity Drives the Acquisition of Goal-Directed Action. *Curr Biol* (2020). https://doi.org/10.1016/j.cub.2020.08.090

109 Ugolini, A., Sokal, D. M., Arban, R. & Large, C. H. CRF1 receptor activation increases the response of neurons in the basolateral nucleus of the amygdala to afferent stimulation. *Front Behav Neurosci* **2**, 2 (2008). https://doi.org/10.3389/neuro.08.002.2008

110 Liu, Z. P. *et al.* Chronic stress impairs GABAergic control of amygdala through suppressing the tonic GABAA receptor currents. *Mol Brain* **7**, 32 (2014). https://doi.org/10.1186/1756-6606-7-32

111 Rosenkranz, J. A., Venheim, E. R. & Padival, M. Chronic stress causes amygdala hyperexcitability in rodents. *Biol Psychiatry* **67**, 1128-1136 (2010). https://doi.org/10.1016/j.biopsych.2010.02.008

112 Hetzel, A. & Rosenkranz, J. A. Distinct effects of repeated restraint stress on basolateral amygdala neuronal membrane properties in resilient adolescent and adult rats. *Neuropsychopharmacology* **39**, 2114-2130 (2014). https://doi.org/10.1038/npp.2014.60

113 Rau, A. R., Chappell, A. M., Butler, T. R., Ariwodola, O. J. & Weiner, J. L. Increased Basolateral Amygdala Pyramidal Cell Excitability May Contribute to the Anxiogenic Phenotype Induced by Chronic Early-Life Stress. *J Neurosci* **35**, 9730-9740 (2015). https://doi.org/10.1523/JNEUROSCI.0384-15.2015

114 Sharp, B. M. Basolateral amygdala and stress-induced hyperexcitability affect motivated behaviors and addiction. *Transl Psychiatry* **7**, e1194 (2017). https://doi.org/10.1038/tp.2017.161

115 Masneuf, S. *et al.* Glutamatergic mechanisms associated with stress-induced amygdala excitability and anxiety-related behavior. *Neuropharmacology* **85**, 190-197 (2014). https://doi.org/10.1016/j.neuropharm.2014.04.015

116 Lowery-Gionta, E. G. *et al.* Chronic stress dysregulates amygdalar output to the prefrontal cortex. *Neuropharmacology* **139**, 68-75 (2018). https://doi.org/10.1016/j.neuropharm.2018.06.032

117 Blume, S. R., Padival, M., Urban, J. H. & Rosenkranz, J. A. Disruptive effects of repeated stress on basolateral amygdala neurons and fear behavior across the estrous cycle in rats. *Sci Rep* **9**, 12292 (2019). https://doi.org/10.1038/s41598-019-48683-3

118 McDonald, A. J. Projection neurons of the basolateral amygdala: a correlative Golgi and retrograde tract tracing study. *Brain Res Bull* **28**, 179-185 (1992).

119 Hunnicutt, B. J. *et al.* A comprehensive excitatory input map of the striatum reveals novel functional organization. *Elife* **5** (2016). https://doi.org/10.7554/eLife.19103

120 Mulder, A. B., Hodenpijl, M. G. & Lopes da Silva, F. H. Electrophysiology of the hippocampal and amygdaloid projections to the nucleus accumbens of the rat: convergence, segregation, and interaction of inputs. *J Neurosci* **18**, 5095-5102 (1998).

121 Shan, Q., Ge, M., Christie, M. J. & Balleine, B. W. The acquisition of goal-directed actions generates opposing plasticity in direct and indirect pathways in dorsomedial striatum. *J Neurosci* **34**, 9196-9201 (2014). https://doi.org/10.1523/JNEUROSCI.0313-14.2014

122 Peak, J., Chieng, B., Hart, G. & Balleine, B. W. Striatal direct and indirect pathway neurons differentially control the encoding and updating of goal-directed learning. *Elife* **9** (2020). https://doi.org/10.7554/eLife.58544

123 Gremel, C. M. & Costa, R. M. Orbitofrontal and striatal circuits dynamically encode the shift between goal-directed and habitual actions. *Nat Commun* **4**, 2264 (2013). https://doi.org/10.1038/ncomms3264

124 Vandaele, Y., Ottenheimer, D. J. & Janak, P. H. Dorsomedial Striatal Activity Tracks Completion of Behavioral Sequences in Rats. *eNeuro* **8** (2021). https://doi.org/10.1523/ENEURO.0279-21.2021

125 Lobo, M. K. & Nestler, E. J. The striatal balancing act in drug addiction: distinct roles of direct and indirect pathway medium spiny neurons. *Front Neuroanat* **5**, 41 (2011). https://doi.org/10.3389/fnana.2011.00041

126 Partridge, J. G. *et al.* Stress increases GABAergic neurotransmission in CRF neurons of the central amygdala and bed nucleus stria terminalis. *Neuropharmacology* **107**, 239-250 (2016). https://doi.org/10.1016/j.neuropharm.2016.03.029

127 Hoffman, A. N., Lorson, N. G., Sanabria, F., Foster Olive, M. & Conrad, C. D. Chronic stress disrupts fear extinction and enhances amygdala and hippocampal Fos expression in an animal model of post-traumatic stress disorder. *Neurobiol Learn Mem* **112**, 139-147 (2014). https://doi.org/10.1016/j.nlm.2014.01.018

128 Patel, S., Cravatt, B. F. & Hillard, C. J. Synergistic interactions between cannabinoids and environmental stress in the activation of the central amygdala. *Neuropsychopharmacology* **30**, 497-507 (2005). https://doi.org/10.1038/sj.npp.1300535

129 He, F., Ai, H., Wang, M., Wang, X. & Geng, X. Altered Neuronal Activity in the Central Nucleus of the Amygdala Induced by Restraint Water-Immersion Stress in Rats. *Neurosci Bull* **34**, 1067-1076 (2018). https://doi.org/10.1007/s12264-018-0282-y

130 Giovanniello, J. *et al.* A Central Amygdala-Globus Pallidus Circuit Conveys Unconditioned Stimulus-Related Information and Controls Fear Learning. *J Neurosci* **40**, 9043-9054 (2020). https://doi.org/10.1523/JNEUROSCI.2090-20.2020

131 Yang, T. *et al.* Plastic and stimulus-specific coding of salient events in the central amygdala. *Nature* **616**, 510-519 (2023). https://doi.org/10.1038/s41586-023-05910-2

132 Wang, Y. *et al.* Multimodal mapping of cell types and projections in the central nucleus of the amygdala. *Elife* **12** (2023). https://doi.org/10.7554/eLife.84262

133 Liu, J. *et al.* Differential efferent projections of GABAergic neurons in the basolateral and central nucleus of amygdala in mice. *Neurosci Lett* **745**, 135621 (2021). https://doi.org/10.1016/j.neulet.2020.135621

134 Sah, P., Faber, E. S., Lopez De Armentia, M. & Power, J. The amygdaloid complex: anatomy and physiology. *Physiol Rev* **83**, 803-834 (2003). https://doi.org/10.1152/physrev.00002.2003

135 Lee, H. J., Gallagher, M. & Holland, P. C. The central amygdala projection to the substantia nigra reflects prediction error information in appetitive conditioning. *Learn Mem* **17**, 531-538 (2010). https://doi.org/10.1101/lm.1889510

136 Kong, M. S. & Zweifel, L. S. Central amygdala circuits in valence and salience processing. *Behav Brain Res* **410**, 113355 (2021). https://doi.org/10.1016/j.bbr.2021.113355

137 Murray, J. E. *et al.* Basolateral and central amygdala differentially recruit and maintain dorsolateral striatum-dependent cocaine-seeking habits. *Nat Commun* **6**, 10088 (2015). https://doi.org/10.1038/ncomms10088

138 Siemsen, B. M., Franco, D. & Lobo, M. K. Corticostriatal contributions to dysregulated motivated behaviors in stress, depression, and substance use disorders. *Neurosci Res* (2022). https://doi.org/10.1016/j.neures.2022.12.014

139 Balleine, B. W. & Killcross, S. Parallel incentive processing: an integrated view of amygdala function. *Trends Neurosci* **29**, 272-279 (2006).

140 Namburi, P. *et al.* A circuit mechanism for differentiating positive and negative associations. *Nature* **520**, 675-678 (2015). https://doi.org/10.1038/nature14366

141 Tye, K. M. Neural Circuit Motifs in Valence Processing. *Neuron* **100**, 436-452 (2018). https://doi.org/10.1016/j.neuron.2018.10.001

142 Gremel, C. M. *et al.* Endocannabinoid Modulation of Orbitostriatal Circuits Gates Habit Formation. *Neuron* **90**, 1312-1324 (2016). https://doi.org/10.1016/j.neuron.2016.04.043

143 Whitelaw, R. B., Markou, A., Robbins, T. W. & Everitt, B. J. Excitotoxic lesions of the basolateral amygdala impair the acquisition of cocaine-seeking behaviour under a second-order schedule of reinforcement. *Psychopharmacology (Berl)* **127**, 213-224 (1996).

144 Alderson, H. L., Robbins, T. W. & Everitt, B. J. The effects of excitotoxic lesions of the basolateral amygdala on the acquisition of heroin-seeking behaviour in rats. *Psychopharmacology (Berl)* **153**, 111-119 (2000).

145 Belin-Rauscent, A., Everitt, B. J. & Belin, D. Intrastriatal shifts mediate the transition from drug-seeking actions to habits. *Biol Psychiatry* **72**, 343-345 (2012). https://doi.org/10.1016/j.biopsych.2012.07.001

146 Murray, J. E., Belin, D. & Everitt, B. J. Double dissociation of the dorsomedial and dorsolateral striatal control over the acquisition and performance of cocaine seeking. *Neuropsychopharmacology* **37**, 2456-2466 (2012). https://doi.org/10.1038/npp.2012.104

147 Roberts, A. J., Cole, M. & Koob, G. F. Intra-amygdala muscimol decreases operant ethanol self-administration in dependent rats. *Alcohol Clin Exp Res* **20**, 1289-1298 (1996).

148 Corbit, L. H., Nie, H. & Janak, P. H. Habitual alcohol seeking: time course and the contribution of subregions of the dorsal striatum. *Biol Psychiatry* **72**, 389-395 (2012). https://doi.org/10.1016/j.biopsych.2012.02.024

149 Wendler, E. *et al.* The roles of the nucleus accumbens core, dorsomedial striatum, and dorsolateral striatum in learning: performance and extinction of Pavlovian fear-conditioned responses and instrumental avoidance responses. *Neurobiol Learn Mem* **109**, 27-36 (2014). https://doi.org/10.1016/j.nlm.2013.11.009

150 Weera, M. M., Schreiber, A. L., Avegno, E. M. & Gilpin, N. W. The role of central amygdala corticotropin-releasing factor in predator odor stress-induced avoidance behavior and escalated alcohol drinking in rats. *Neuropharmacology* **166**, 107979 (2020). https://doi.org/10.1016/j.neuropharm.2020.107979

151 Marti-Prats, L. *et al.* Baclofen decreases compulsive alcohol drinking in rats characterized by reduced levels of GAT-3 in the central amygdala. *Addict Biol* **26**, e13011 (2021). https://doi.org/10.1111/adb.13011

152 Franklin, K. B. J. & Paxinos, G. *The Mouse Brain in Stereotaxic Coordinates*. 3rd Edition edn, (Elsevier, 2008).

153 Tye, K. M. *et al.* Dopamine neurons modulate neural encoding and expression of depression-related behaviour. *Nature* **493**, 537-541 (2013). https://doi.org/10.1038/nature11740

154 Cerniauskas, I. *et al.* Chronic Stress Induces Activity, Synaptic, and Transcriptional Remodeling of the Lateral Habenula Associated with Deficits in Motivated Behaviors. *Neuron* **104**, 899-915.e898 (2019). https://doi.org/10.1016/j.neuron.2019.09.005

155 Monteiro, S. *et al.* An efficient chronic unpredictable stress protocol to induce stress-related responses in C57BL/6 mice. *Front Psychiatry* **6**, 6 (2015). https://doi.org/10.3389/fpsyt.2015.00006

156 Bavley, C. C., Fischer, D. K., Rizzo, B. K. & Rajadhyaksha, A. M. Ca. *Neurobiol Stress* **7**, 27-37 (2017). https://doi.org/10.1016/j.ynstr.2017.02.004

157 Freymann, J., Tsai, P. P., Stelzer, H. D., Mischke, R. & Hackbarth, H. Impact of bedding volume on physiological and behavioural parameters in laboratory mice. *Lab Anim* **51**, 601-612 (2017). https://doi.org/10.1177/0023677217694400

158 Pałucha-Poniewiera, A., Podkowa, K., Rafało-Ulińska, A., Brański, P. & Burnat, G. The influence of the duration of chronic unpredictable mild stress on the behavioural responses of C57BL/6J mice. *Behav Pharmacol* **31**, 574-582 (2020). https://doi.org/10.1097/FBP.0000000000000564

159 La-Vu, M. Q. *et al.* Sparse genetically defined neurons refine the canonical role of periaqueductal gray columnar organization. *Elife* **11** (2022). https://doi.org/10.7554/eLife.77115

160 Reis, F. M. *et al.* Dorsal periaqueductal gray ensembles represent approach and avoidance states. *Elife* **10** (2021). https://doi.org/10.7554/eLife.64934

161 Lichtenberg, N. T. *et al.* The Medial Orbitofrontal Cortex-Basolateral Amygdala Circuit Regulates the Influence of Reward Cues on Adaptive Behavior and Choice. *J Neurosci* **41**, 7267-7277 (2021). https://doi.org/10.1523/JNEUROSCI.0901-21.2021

162 Sias, A. *et al.* A bidirectional corticoamygdala circuit for the encoding and retrieval of detailed reward memories. *eLife* **10** (2021). https://doi.org/DOI: 10.7554/eLife.68617

163 Sherathiya, V. N., Schaid, M. D., Seiler, J. L., Lopez, G. C. & Lerner, T. N. GuPPy, a Python toolbox for the analysis of fiber photometry data. *Sci Rep* **11**, 24212 (2021). https://doi.org/10.1038/s41598-021-03626-9

164 Roth, B. L. DREADDs for Neuroscientists. *Neuron* **89**, 683-694 (2016). https://doi.org/10.1016/j.neuron.2016.01.040

165 Pomrenze, M. B. *et al.* A Corticotropin Releasing Factor Network in the Extended Amygdala for Anxiety. *J Neurosci* **39**, 1030-1043 (2019). https://doi.org/10.1523/JNEUROSCI.2143-18.2018

166 Malvaez, M., Shieh, C., Murphy, M. D., Greenfield, V. Y. & Wassum, K. M. Distinct cortical–amygdala projections drive reward value encoding and retrieval. *Nature Neuroscience* (2019). https://doi.org/10.1038/s41593-019-0374-7

167 Collins, A. L. *et al.* Nucleus Accumbens Cholinergic Interneurons Oppose Cue-Motivated Behavior. *Biol Psychiatry* (2019). https://doi.org/10.1016/j.biopsych.2019.02.014

168 Lichtenberg, N. T. *et al.* The medial orbitofrontal cortex - basolateral amygdala circuit regulates the influence of reward cues on adaptive behavior and choice. *J Neurosci* (2021). https://doi.org/10.1523/JNEUROSCI.0901-21.2021

169 Schmider, E., Ziegler, M., Danay, E., Beyer, L. & Bühner, M. Is it really robust? Reinvestigating the robustness of ANOVA against violations of the normal distribution assumption. *Methodology : European journal of research methods for the behavioral & social sciences* **6**, 147-151 (2010).

170 Knief, U. & Forstmeier, W. Violating the normality assumption may be the lesser of two evils. *Behav Res Methods* **53**, 2576-2590 (2021). https://doi.org/10.3758/s13428-021-01587-5

171 Malvaez, M. *et al.* Habits are negatively regulated by HDAC3 in the dorsal striatum. *bioRxiv* (2017). https://doi.org/https://doi.org/10.1101/153734

172 Wassum, K. *et al.* (Dryad, 2021).

173 Mineur, Y. S., Belzung, C. & Crusio, W. E. Effects of unpredictable chronic mild stress on anxiety and depression-like behavior in mice. *Behav Brain Res* **175**, 43-50 (2006). https://doi.org/10.1016/j.bbr.2006.07.029

174 Fang, X. *et al.* Chronic unpredictable stress induces depression-related behaviors by suppressing AgRP neuron activity. *Mol Psychiatry* **26**, 2299-2315 (2021). https://doi.org/10.1038/s41380-020-01004-x

175 Gong, S. *et al.* Targeting Cre recombinase to specific neuron populations with bacterial artificial chromosome constructs. *J Neurosci* **27**, 9817-9823 (2007). https://doi.org/10.1523/JNEUROSCI.2707-07.2007

176 Valjent, E., Bertran-Gonzalez, J., Hervé, D., Fisone, G. & Girault, J. A. Looking BAC at striatal signaling: cell-specific analysis in new transgenic mice. *Trends Neurosci* **32**, 538-547 (2009). https://doi.org/10.1016/j.tins.2009.06.005

SUPPLEMENTAL FIGURES AND TABLES

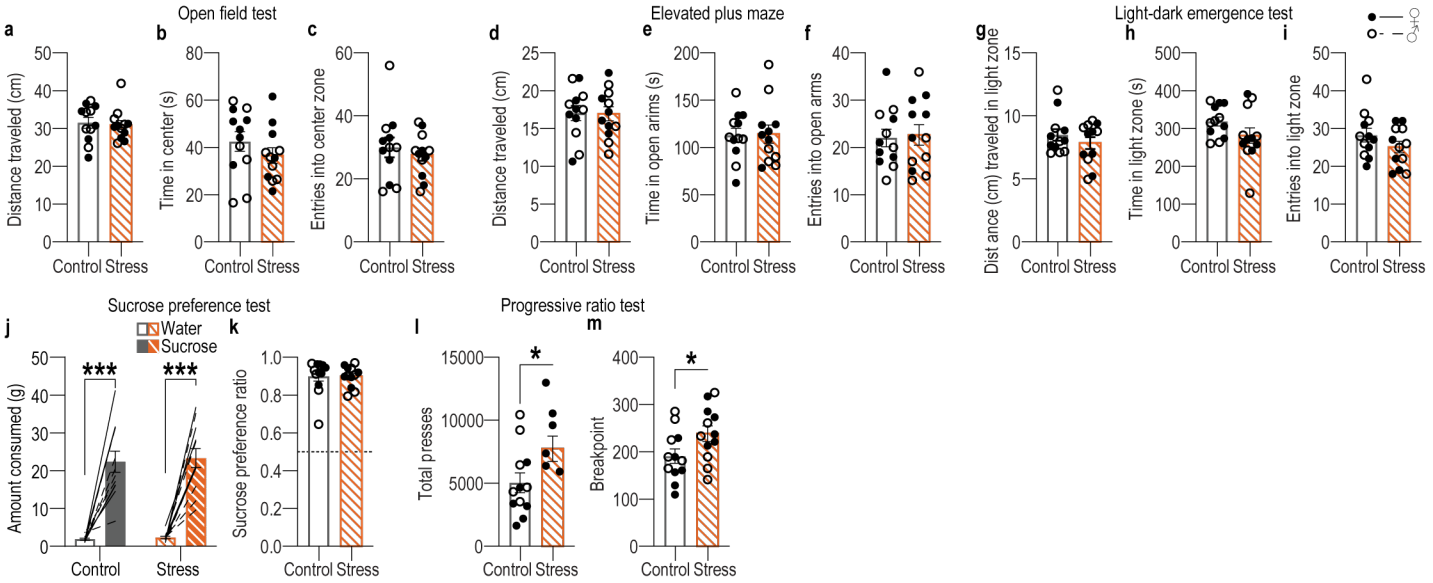

Supplemental Figure 1-1: Chronic mild unpredictable stress does not cause classic anxiety- and depression-like phenotypes. Mice received 14 consecutive d of chronic mild unpredictable stress (CUS) including twice daily exposure to 1 of 6 mild stressors at pseudorandom times and orders: damp bedding (16 hr), tilted cage (16 hr), white noise (80 db; 2 hr), continuous illumination (8 hr), physical restraint (2 hr), footshock (0.7-mA, 1-s, 5 shocks/10 min) prior to subsequent testing in a battery of behavioral assays classically used to assess anxiety- and depression-like behavior. **(a-c)** Distance traveled (a; $t_{(22)} = 0.32$, $P = 0.75$), time spent in center zone (b; $t_{(22)} = 1.10$, $P = 0.28$), and entries into center zone (c; $t_{(22)} = 0.63$, $P = 0.54$) of the open field test. **(d-f)** Distance traveled (d; $t_{(22)} = 0.08$, $P = 0.94$), time spent in open arms (e; $t_{(22)} = 0.01$, $P = 0.92$), and entries into open arms (f; $t_{(22)} = 0.23$, $P = 0.82$) of the elevated plus maze. **(g-i)**, Distance traveled in light zone (g; $t_{(22)} = 0.97$, $P = 0.34$), time spent in light zone (h; $t_{(22)} = 1.57$, $P = 0.13$), and entries into light zone (I; $t_{(22)} = 1.37$, $P = 0.19$) of light-dark emergence test. **(j-k)** Average amount consumed of water and 10% sucrose over 24 hr (j; Solution: $F_{(1, 22)} = 113.20$, $P < 0.0001$; Stress: $F_{(1, 22)} = 0.14$, $P = 0.71$, Solution x Stress: $F_{(1, 22)} = 0.02$, P = 0.89) and ratio of sucrose:water consumed (k; $t_{(22)} = 0.03$, $P = 0.98$) during the sucrose preference test. **(l-m)** Total presses (l; $t_{(22)} = 2.13$, $P = 0.04$) and breakpoint (k; Final ratio completed; $t_{(22)} = 2.12$, $P = 0.46$) during the progressive ratio test. Control N = 12 (6 male), Stress N = 12 (6 male). Males = closed circles, Females = open circles. *P <0.05, ***P <0.001. Our CUS procedure does not affect general locomotor activity or avoidance of anxiogenic spaces or create an anhedonia phenotype. Rather this CUS procedure appears to cause elevated motivation to exert effort to obtain reward. This contrasts with more severe, longer-lasting CUS procedures, which do produce anxiety- and depression-like phenotypes in these tasks[155,173,174]. Thus, our CUS procedure models chronic, low-level stress.

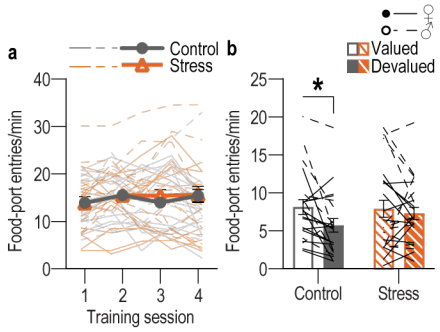

Supplemental Figure 1-2: Food-port entries during training and devaluation probe tests following handling control or chronic stress. (a) Food-port entry rate across training following CUS (Stress) or daily handling control. Training: $F_{(2.42, 108.90)} = 3.17$, $P = 0.04$; Stress: $F_{(1, 45)} = 0.07$, $P = 0.79$; Training x Stress: $F_{(3, 135)} = 0.57$, $P = 0.64$. **(b)** Food-port entries during the subsequent devaluation probe tests. Value: $F_{(1, 45)} = 6.77$, $P = 0.01$, Stress: $F_{(1, 45)} = 0.29$, $P = 0.60$; Stress x Value: $F_{(1, 45)} = 2.42$, $P = 0.13$. Control N = 22 (13 male), Stress N = 25 (12 male). Males = solid lines, Females = dashed lines. *$P < 0.05$.

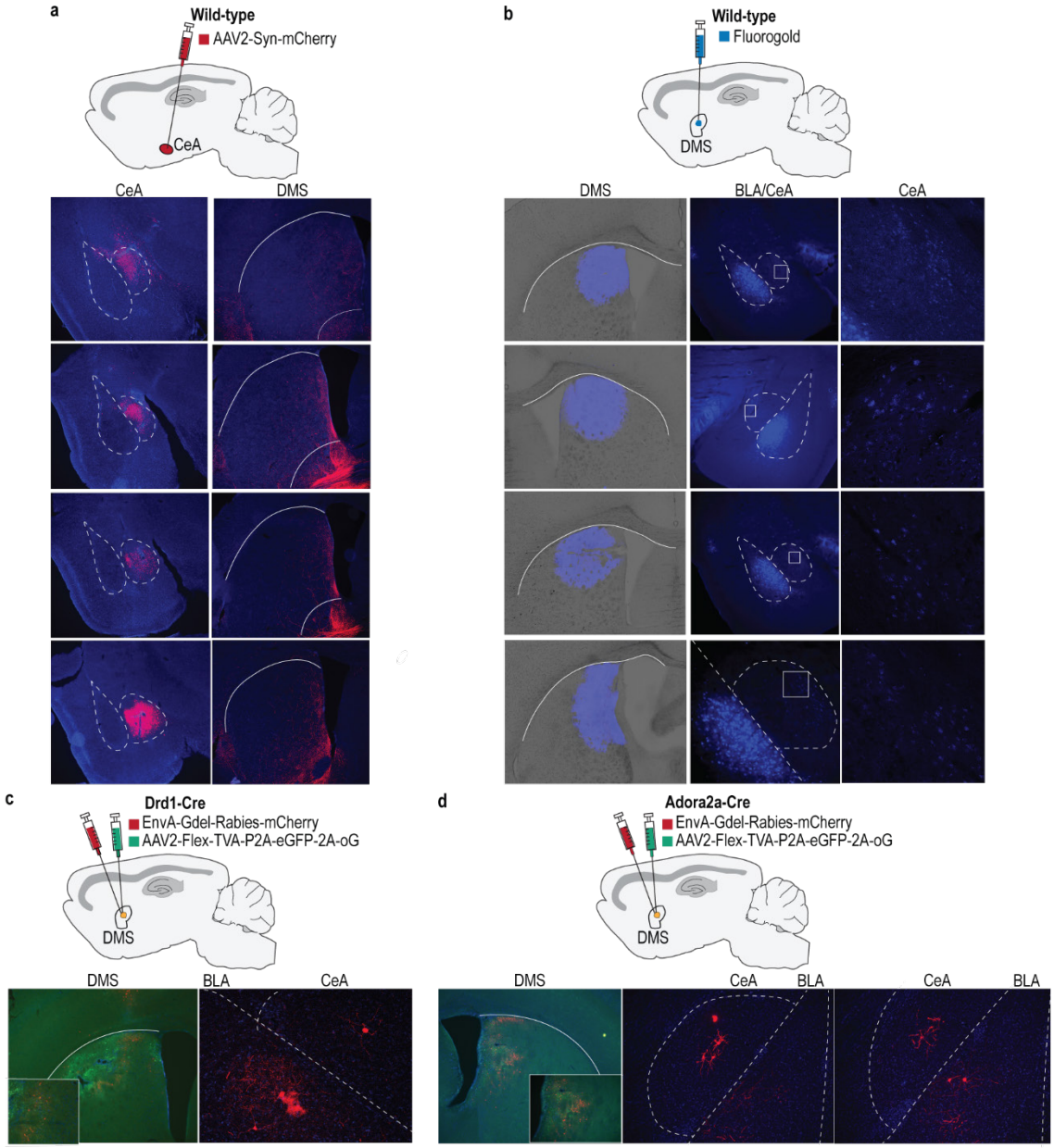

Supplemental Figure 2: BLA and CeA directly project to DMS. (a) Top: Anterograde tracing approach. Infusion of an AAV expressing mCherry into the CeA. Bottom: mCherry labeling at infusion site in CeA (left) and mCherry-labeled fibers in the DMS (right). N = 4 (2 male). We observed mCherry-expressing putative fibers in the DMS but not dorsolateral striatum. Expression was also detected in other well-known CeA projection targets such as the bed nucleus of the stria terminalis. **(b)** Top: Retrograde tracing approach. We infused the fluorescently labeled retrograde tracer Fluorogold into the DMS. Bottom: Fluorogold labeling at infusion site in DMS (left) and fluorogold-labeled, DMS-projecting cell bodies in BLA and CeA (middle), with CeA magnified (right). Labeled cells was detected in both BLA and CeA, indicating that both BLA and CeA directly project to DMS. Labeling was greater in BLA than CeA, indicating the BLA→DMS pathway is denser than the CeA→DMS pathway. N = 4 (2 male). **(c)** Top: Approach for rabies trans-synaptic retrograde tracing of DMS Drd1$^+$ striatal neurons. We used rabies tracing to confirm monosynaptic amygdala projections onto DMS neurons. We infused a starter virus expressing cre-dependent TVA-oG-GFP into the DMS of mice expressing cre-recombinase under the control of dopamine receptor 1 (D1-Cre) or adenosine 2a receptor (A2A-Cre) genes[175,176], followed by ΔG-deleted rabies-mCherry to retrogradely label cells that synapse onto DMS D1 or A2A neurons. Bottom: Starter oG virus (green) and ΔG-deleted rabies-mCherry (red) expression in DMS Drd1$^+$ neurons (left) and rabies-labeled, DMS D1-projecting cell bodies in the BLA and CeA (right), consistent with prior reports[80,81]. Representative example from N = 4 (3 males). **(d)** Top: Approach for rabies trans-synaptic retrograde tracing of DMS Adora2a$^+$ neurons. Bottom: Starter ΔG virus (green) and rabies-mCherry (red) expression in DMS Adora2a$^+$

neurons (left) and rabies-labeled, DMS A2A-projecting cell bodies in the BLA and CeA (right). Representative example N = 4 (3 males). Combined, these data confirm that both BLA and CeA directly project to the DMS and are, thus, poised to influence the learning that supports goal-directed behavioral control and habit formation.

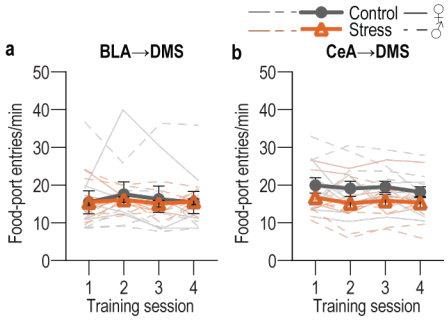

Supplemental Figure 2-1: Food-port entries during training with fiber photometry recording of BLA→DMS or CeA→DMS calcium activity following handling control or chronic stress. (a) Food-port entry rates across training for BLA→DMS GCaMP8s mice following CUS (Stress) or daily handling control. Training: $F_{(2.47, 46.99)} = 0.65$, $P = 0.56$; Stress: $F_{(1, 19)} = 0.05$, $P = 0.82$; Training x Stress: $F_{(3, 57)} = 0.24$, $P = 0.87$. BLA Control N = 9 (4 male), BLA Stress N = 12 (5 male). **(b)** Food-port entry rates across training for CeA→DMS GCaMP8s mice following CUS or daily handling control. Training: $F_{(2.36, 47.19)} = 0.89$, $P = 0.43$; Stress: $F_{(1, 20)} = 2.71$, $P = 0.12$; Training x Stress: $F_{(3, 60)} = 0.09$, $P = 0.96$. CeA Control N = 11 (6 male), CeA Stress N = 11 (4 male). Males = solid lines, Females = dashed lines.

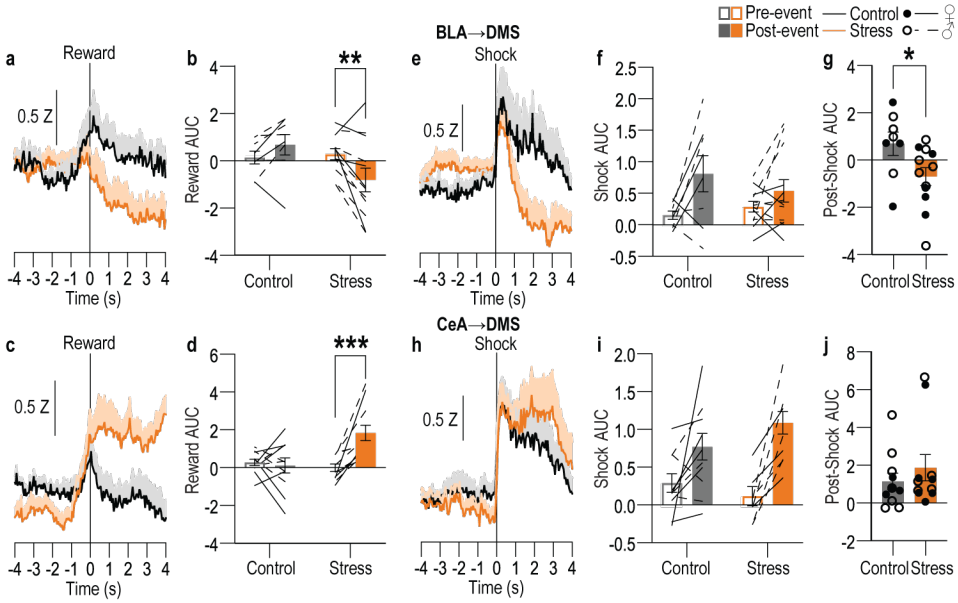

Supplemental Figure 2-2: BLA→DMS and CeA→DMS pathway responses to unpredicted rewarding and aversive events in control and stressed mice. Following instrumental training (Figure 2), we used fiber photometry to record GCaMP8s fluorescent changes in either BLA (top) or CeA (bottom) neurons that project to the DMS in response to unpredicted food-pellet reward deliveries or unpredicted 2-s, 0.7 mA footshocks in control and stressed mice. **(a)** Trial-averaged Z-scored Δf/F BLA→DMS GCaMP8s fluorescence changes around unpredicted food-pellet reward delivery. **(b)** Trial-averaged quantification of area under the BLA→DMS GCaMP8s Z-scored Δf/F curve (AUC) during the 3-s period prior to (baseline) and following reward collection. Stress x Reward: $F_{(1, 18)} = 10.88$, $P = 0.004$; Reward: $F_{(1, 18)} = 1.19$; $P = 0.03$; Stress: $F_{(1, 18)} = 1.77$, $P = 0.20$. **(c)** Trial-averaged Z-scored Δf/F CeA→DMS GCaMP8s fluorescence changes around unpredicted food-pellet reward delivery. **(d)** Trial-averaged quantification CeA→DMS GCaMP8s Z-scored Δf/F AUC during the 3-s period prior to and following reward collection. Stress x Reward: $F_{(1, 20)} = 11.79$, $P = 0.02$; Reward: $F_{(1, 20)} = 8.14$, $P = 0.01$; Stress $F_{(1, 20)} = 4.49$, $P = 0.05$. **(e)** Trial-averaged Z-scored Δf/F BLA→DMS GCaMP8s fluorescence changes around unpredicted footshock. **(f)** Trial-averaged quantification of BLA→DMS GCaMP8s Z-scored Δf/F AUC during the 1-s acute shock response compared to a 1-s pre-shock baseline. Shock: $F_{(1, 18)} = 8.533$, $P = 0.01$; Stress: $F_{(1, 18)} = 0.1433$, $P = 0.71$; Stress x Shock $F_{(1, 18)} = 1.725$, $P = 0.21$ **(g)** Trial-averaged quantification of BLA→DMS GCaMP8s Z-scored Δf/F AUC during 2-s post-shock period. $t_{(18)} = 2.26$, $P = 0.04$. **(h)** Trial-averaged Z-scored Δf/F CeA→DMS GCaMP8s fluorescence changes around unpredicted footshock. **(i)** Trial-averaged quantification of CeA→DMS GCaMP8s Z-scored Δf/F AUC during the 1-s acute shock response, compared to baseline. Shock: $F_{(1, 20)} = 28.24$, $P < 0.0001$; Stress: $F_{(1, 20)} = 0.22$, $P = 0.64$; Stress x Shock: $F_{(1, 20)} = 3.201$, $P = 0.09$. **(j)** Trial-averaged quantification of CeA→DMS GCaMP8s Z-scored Δf/F AUC during 2-s post-shock period. $t_{(20)} = 0.8798$, $P = 0.39$. BLA Control N = 8 (4 male), BLA Stress N = 12 (5 male). CeA Control N = 11 (6 male), CeA Stress N = 11 (4 male). Males = solid lines, Females = dashed lines. BLA→DMS projections are activated by unpredicted rewards and this is attenuated by prior chronic stress. Conversely, CeA→DMS projections are not normally robustly activated by unpredicted rewards, but are activated by unpredicted rewards following chronic stress. Both BLA→DMS and CeA→DMS pathways are acutely activated by unpredicted footshock regardless of prior stress. Though chronic stress reduces post-shock activity in the BLA→DMS pathway.

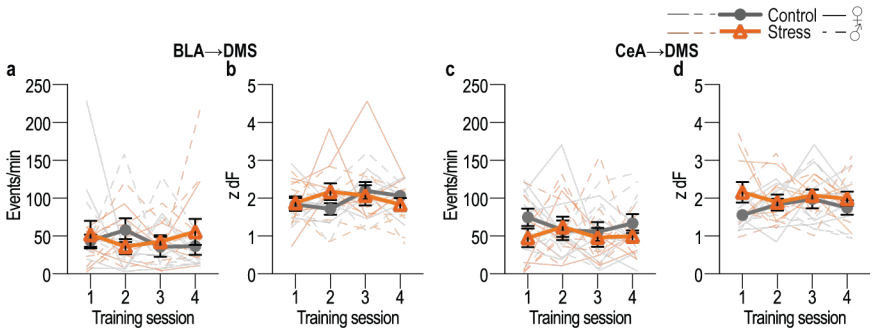

Supplemental Figure 2-3: Chronic stress does not affect spontaneous calcium activity in BLA→DMS or CeA→DMS projections. (a-b) Frequency (a; Training: $F_{(2.41, 45.69)} = 0.17$, $P = 0.88$; Stress: $F_{(1, 19)} = 0.08$, $P = 0.78$; Training x Stress: $F_{(3, 57)} = 0.85$, P = 0.47) and amplitude (b; Training: $F_{(2.48, 47.10)} = 0.86$, $P = 0.45$; Stress: $F_{(1, 19)} = 0.034$, $P = 0.85$; Training x Stress: $F_{(3, 57)} = 1.37$, $P = 0.26$) of Z-scored Δf/F spontaneous calcium activity of BLA→DMS projections during the 3-min baseline period prior to each training session in handled control and stressed mice. **(c-d)** Frequency (c; Training: $F_{(2.70, 53.97)} = 0.21$, $P = 0.88$; Stress $F_{(1, 20)} = 3.03$, $P = 0.10$; Training x Stress: $F_{(3, 60)} = 0.55$, $P = 0.65$) and amplitude (d; Training: $F_{(2.59, 51.83)} = 0.32$, $P = 0.78$; Stress: $F_{(1, 20)} = 3.70$, $P = 0.07$; Training x Stress: $F_{(3, 60)} = 0.75$, $P = 0.52$) of Z-scored Δf/F spontaneous calcium activity of CeA→DMS projections during the 3-min baseline period prior to each training session handled control and stressed mice. Males = solid lines, Females = dashed lines. Chronic stress did not alter baseline spontaneous calcium activity in either pathway.

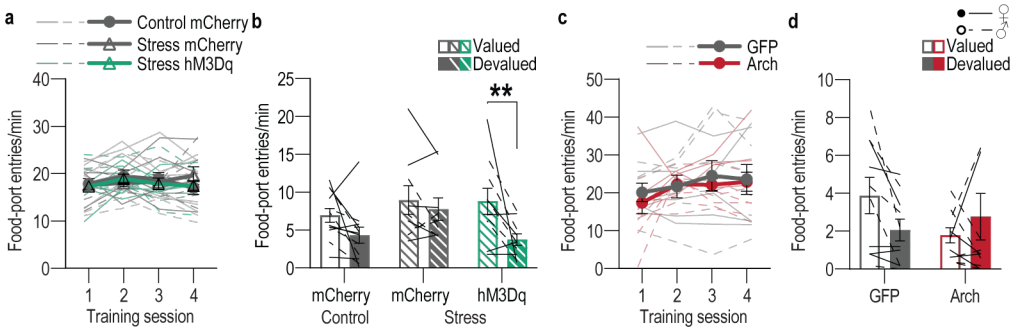

Supplemental Figure 3-1: Food-port entries during training with BLA→DMS manipulations and devaluation probe tests. (a-b) Chemogenetic activation of BLA→DMS projections during post-stress instrumental learning. **(a)** Food-port entry rate across training following CUS (Stress) or daily handling control. Training: $F_{(2.4, 68.12)} = 1.20$, $P = 0.31$; Group: $F_{(2, 28)} = 0.06$, $P = 0.94$; Training x Group: $F_{(6, 84)} = 1.23$, $P = 0.30$. **(b)** Food-port entry rate during the subsequent devaluation probe test immediately following sensory-specific satiety devaluation of the trained pellet (Devalued condition) or an alternate pellet type (Valued condition). Value: $F_{(1, 28)} = 13.36$, $P = 0.001$; Group: $F_{(2, 28)} = 1.60$, $P = 0.22$; Group x Value: $F_{(2, 28)} = 1.85$, $P = 0.18$. Control mCherry N = 12 (7 male), Stress mCherry N = 9 (5 male), Stress hM3Dq N = 10 Stress (5 male). **(c-d)** Optogenetic inactivation of BLA→DMS projections at reward during instrumental learning. **(c)** Food-port entries across training. Training: $F_{(2.03, 38.55)} = 3.30$, $P = 0.05$; Virus: $F_{(1, 19)} = 0.14$, $P = 0.71$; Training x Virus: $F_{(3, 57)} = 0.43$, $P = 0.73$. **(d)** Food-port entry rates during subsequent devaluation probe tests. Stress x Value: $F_{(1, 19)} = 4.38$, $P = 0.05$; Stress: $F_{(1, 19)} = 0.47$, $P = 0.50$; Value: $F_{(1, 19)} = 0.39$, $P = 0.54$. GFP N = 10 (5 males), Arch N = 11 (5 male). Males = solid lines, Females = dashed lines. $^{**}P < 0.01$.

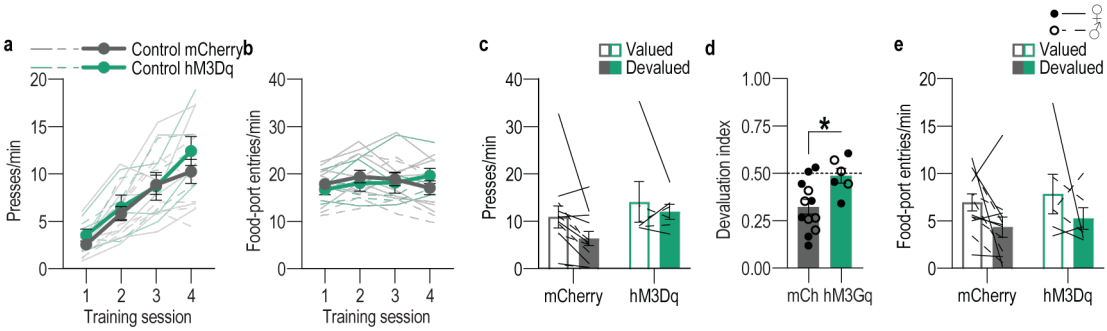

Supplemental Figure 3-2: Effect of BLA→DMS chemogenetic activation on action-outcome learning. Using an intersectional approach (Figure 3a), we expressed the excitatory designer receptor human M3 muscarinic receptor (hM3Dq) or fluorophore control in BLA→DMS neurons. Mice received instrumental training to lever press to earn food-pellet rewards. Prior to each training session, mice received the hM3Dq ligand clozapine-N-oxide (CNO; 0.2 mg/kg i.p.). Press rate across training. Training: $F_{(2.27, 36.30)} = 43.87$, $P < 0.0001$; Virus: $F_{(1, 16)} = 0.50$, $P = 0.49$; Training x Virus: $F_{(3, 48)} = 0.80$, $P = 0.50$. **(b)** Food-port entry rate across training. Training: $F_{(2.57, 41.19)} = 1.18$, $P = 0.33$; Virus: $F_{(1, 16)} = 0.007$, $P = 0.93$. Training x Virus: $F_{(3, 48)} = 2.23$, $P = 0.10$. Chemogenetic activation of BLA→DMS projections did not alter acquisition of the instrumental lever-press behavior. **(c)** Press rate during the subsequent devaluation probe tests immediately following sensory-specific satiety devaluation of the trained pellet (Devalued condition) or an alternate pellet type (Valued condition). Value: $F_{(1, 16)} = 4.11$, $P = 0.06$; Virus: $F_{(1, 16)} = 1.92$ $P = 0.19$; Virus x Value: $F_{(1, 16)} = 0.57$, $P = 0.46$. **(d)** Devaluation index. $t_{(16)} = 2.69$, $P = 0.02$. **(e)** Food-port entry rate during devaluation probe tests. Value: $F_{(1, 16)} = 4.56$, $P = 0.05$; Virus: $F_{(1, 16)} = 0.43$, $P = 0.52$; Virus x Value: $F_{(1, 16)} = 0.0002$, $P = 0.99$. mCherry N = 12 (7 male), hM3Dq N = 6 (3 male). Males = closed circles/solid lines, Females = open circles/dashed lines. *$P < 0.05$. Chemogenetic activation of BLA→DMS projections in subjects without a history of chronic stress slightly promotes habit formation, likely by disrupting the endogenous pattern of activity (see Figure 2d-i) in this pathway that is important for action-outcome learning (see Figure 3h-n).

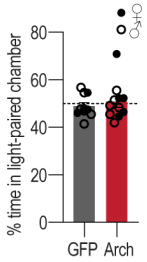

Supplemental Figure 3-3: Inhibition of BLA terminals in DMS is not rewarding or aversive. Following training and testing (Figure 3h-n) mice receive a real-time place preference test in which 1 side of a 2-chamber apparatus was paired with optogenetic inhibition of BLA axons and terminals in the DMS. Average percent time spent in light-paired chamber across 2, 10-minute sessions (one with light paired with each side). $t_{(19)} = 0.65$, $P = 0.5$. GFP N = 10 (5 male), Arch N = 11 (5 male). Males = closed circles, Females = open circles.

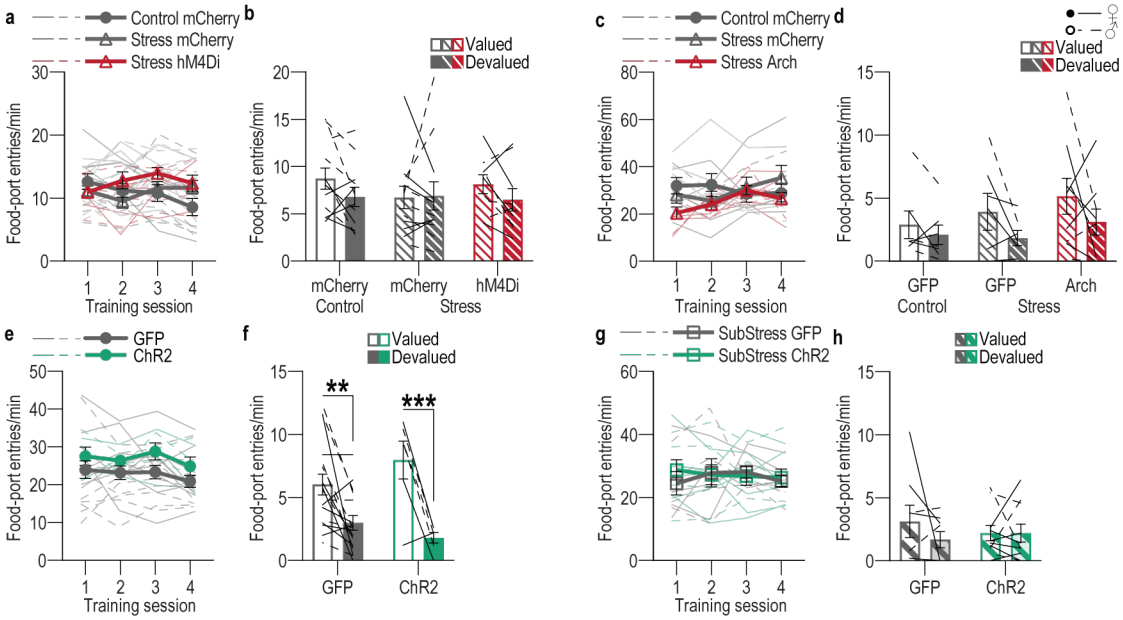

Supplemental Figure 4-1: Food-port entries during training with CeA→DMS manipulations and devaluation probe tests. **(a-b)** Chemogenetic inhibition of CeA→DMS projections during post-stress instrumental learning. **(a)** Food-port entry rates across training following CUS (Stress) or daily handling control. Training: $F_{(1.85, 53.71)} = 1.07$, $P = 0.35$; Group: $F_{(2, 29)} = 1.25$, $P = 0.30$; Training x Group: $F_{(6, 87)} = 2.93$, $P = 0.01$. **(b)** Food-port entry rates during the subsequent devaluation probe tests. Value: $F_{(1, 30)} = 2.65$, $P = 0.11$; Group: $F_{(2, 30)} = 0.23$, $P = 0.80$; Group x Value: $F_{(2, 30)} = 0.96$, $P = 0.40$. Control mCherry N = 12 (5 male), Stress mCherry N = 11 (5 male), Stress hM4Di N = 9 (4 male). **(c-d)** Optogenetic inactivation of CeA→DMS projections at reward during post-stress learning. **(c)** Food-port entry rates across training following CUS or daily handling control. Training x Group: $F_{(6, 60)} = 2.33$, $P = 0.04$; Training: $F_{(2.14, 42.88)} = 1.46$, $P = 0.24$; Group: $F_{(2, 20)} = 1.22$, $P = 0.32$. **(d)** Food-port entry rates during the subsequent devaluation probe tests. Value: $F_{(1, 20)} = 4.73$, $P = 0.04$; Group: $F_{(2, 20)} = 0.89$, $P = 0.43$; Group x Value: $F_{(2, 20)} = 0.30$, $P = 0.74$. Control GFP N = 7 (4 male), Stress GFP N = 7 (6 male), Stress Arch N = 9 (5 male). **(e-f)** Optogenetic stimulation of CeA→DMS projections at reward during learning. **(e)** Food-port entries across training. Training: $F_{(2.42, 50.77)} = 2.00$, $P = 0.14$; Virus: $F_{(1, 21)} = 1.85$, $P = 0.19$; Training x Virus: $F_{(3, 63)} = 0.22$, $P = 0.88$. **(f)** Food-port entries during the subsequent devaluation probe tests. Value: $F_{(1, 21)} = 30.07$, $P < 0.0001$; Virus: $F_{(1, 21)} = 0.12$, $P = 0.73$; Virus x Value: $F_{(1, 21)} = 3.45$, $P = 0.08$. GFP N = 17 (9 male), ChR2 N = 6 (3 male). **(g-h)** Optogenetic stimulation of CeA→DMS projections at reward during learning following subthreshold once daily CUS (SubStress). **(g)** Food-port entry rates across training session following once/daily, 14 d CUS. Training: $F_{(1.47, 23.44)} = 0.24$, $P = 0.72$; Virus: $F_{(1, 16)} = 0.07$, $P = 0.80$; Training x Virus: $F_{(3, 48)} = 0.52$, $P = 0.67$. **(h)** Food-port entry rates the subsequent during devaluation probe tests. Virus: $F_{(1, 16)} = 0.05$, $P = 0.83$; Value: $F_{(1, 16)} = 0.95$, $P = 0.34$; Virus x Value: $F_{(1, 16)} = 0.95$, $P = 0.34$. GFP N = 8 (4 male), ChR2 N = 10 (6 male). Males = solid lines, Females = dashed lines. ** $P < 0.01$, *** $P < 0.001$.

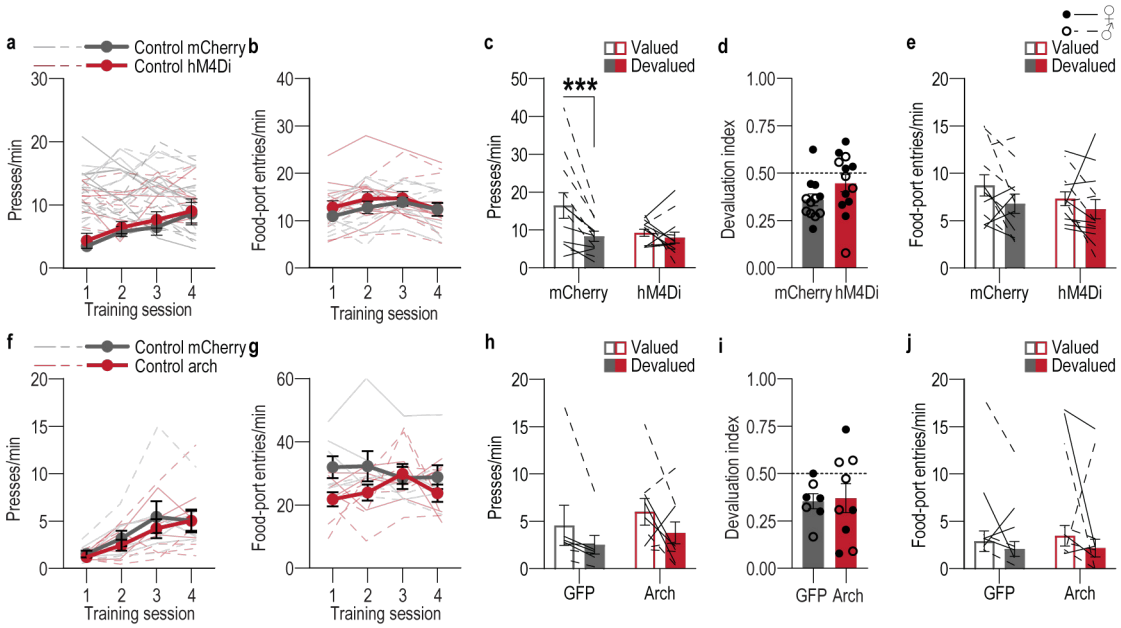

Supplemental Figure 4-2: Effect of CeA→DMS inhibition on action-outcome learning. (a-e) Chemogenetic inhibition of CeA→DMS projections during instrumental learning. Using an intersectional approach (Figure 4a), we expressed the inhibitory designer receptor human M4 muscarinic receptor (hM4Di) or fluorophore control in CeA→DMS neurons. Mice received instrumental training to lever press to earn food pellet rewards. Prior to each training session, mice received the hM4Di ligand clozapine-N-oxide (CNO; 2.0 mg/kg i.p.). **(a)** Press rate across training. Training: $F_{(1.70, 39.13)} = 16.75$, $P < 0.0001$; Virus: $F_{(1, 23)} = 0.22$, $P = 0.65$; Training x Virus: $F_{(3, 69)} = 0.10$, $P = 0.96$. **(b)** Food-port entry rate across training. Training: $F_{(1.85, 42.64)} = 3.35$, $P = 0.05$; Virus: $F_{(1, 23)} = 0.55$, $P = 0.46$; Training x Virus: $F_{(3, 69)} = 0.49$, $P = 0.69$. Chemogenetic inhibition of CeA→DMS projections did not alter acquisition of the instrumental lever-press behavior. **(c)** Press rate during the subsequent devaluation probe tests immediately following sensory-specific satiety devaluation of the trained pellet (Devalued condition) or an alternate pellet type (Valued condition). Virus x Value: $F_{(1, 23)} = 6.72$, $P = 0.02$; Virus: $F_{(1, 23)} = 2.44$, $P = 13$; Value: $F_{(1, 23)} = 12.55$, $P = 002$. **(d)** Devaluation index. $t_{(23)} = 1.58$, $P = 0.13$. **(e)** Food-port entry rate during devaluation probe tests. Value: $F_{(1, 23)} = 5.17$, $P = 0.03$; Virus: $F_{(1, 23)} = 0.69$, $P = 0.04$; Virus x Value: $F_{(1, 23)} = 0.38$; $P = 0.54$. mCherry N = 12 (5 male), hM4Di N = 13 (8 male). Chemogenetic inactivation of CeA→DMS projections slightly disrupted action-outcome learning, likely by altering typical signaling dynamics in this pathway. **(f-j)** Optogenetic inactivation of CeA→DMS projections at reward during post-stress learning. We expressed the inhibitory opsin archaerhodopsin (Arch) or fluorophore control in the CeA and implanted optical fibers in the DMS in the vicinity of Arch-expressing CeA axons and terminals (Figure 4h-j). Mice received instrumental training to lever press to earn food-pellet rewards. We used green light (532 nm, 10 mW, 5 s) to inhibit CeA terminals in the DMS during the collection of each earned reward. **(f)** Press rate across training. Training: $F_{(1.98, 27.70)} = 13.11$, $P = 0.0001$; Virus: $F_{(1, 14)} = 0.28$, $P = 0.60$; Training x Virus: $F_{(3, 42)} = 0.29$, $P = 0.83$. **(g)** Food-port entry rate across training. Training: $F_{(2.57, 35.95)} = 0.57$, $P = 0.61$; Virus: $F_{(1, 14)} = 2.50$, $P = 0.14$; Training x Virus: $F_{(3, 42)} = 2,20$, $P = 0.10$. Optogenetic inhibition of CeA→DMS projections did not alter acquisition of the instrumental lever-press behavior. **(h)** Press rate during the subsequent devaluation probe tests. Value: $F_{(1, 14)} = 4.91$, $P = 0.04$; Virus: $F_{(1, 14)} = 0.55$, $P = 0.47$; Virus x Value: $F_{(1, 14)} = 0.007$, $P = 0.93$. **(i)** Devaluation index. $t_{(14)} = 0.17$, $P = 0.87$. **(j)** Food-port entry rate during devaluation probe tests. Value: $F_{(1, 14)} = 1.77$, $P = 0.20$; Virus $F_{(1, 14)} = 0.08$, $P = 0.78$; Virus x Value: $F_{(1, 14)} = 0.10$, $P = 0.76$. GFP N = 7 (4 male), Arch N = 9 (4 male). Males = closed circles/solid lines, Females = open circles/dashed lines. *** $P < 0.001$. Optogenetic inactivation of CeA→DMS projections did not alter action-outcome learning for goal-directed behavioral control.

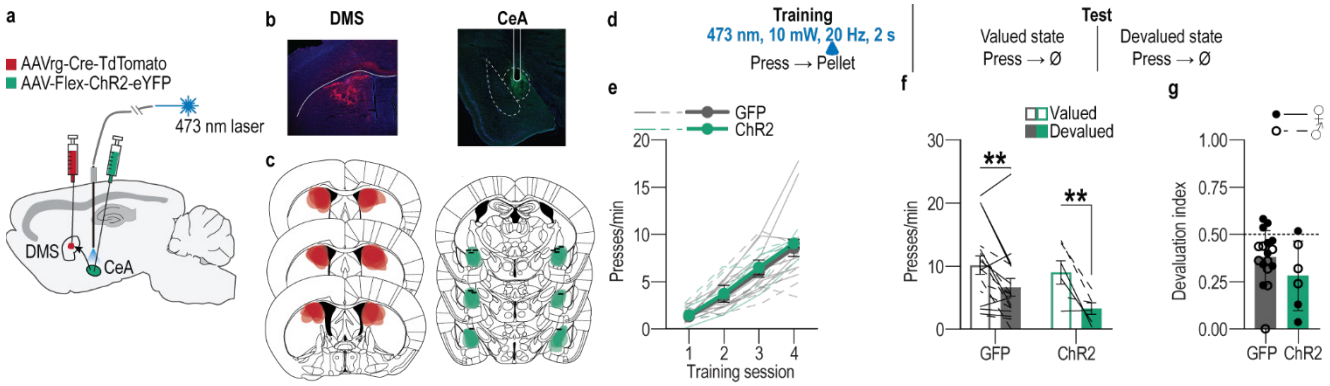

Supplemental Figure 4-3: Optogenetic stimulation of CeA→DMS projections in control mice. (a) We used an intersectional approach to express the excitatory opsin Channelrhodopsin 2 (ChR2), or a fluorophore control in DMS-projecting CeA neurons and implanted optic fibers above the CeA. **(b)** Representative images of retro-cre expression in DMS and immunofluorescent staining of cre-dependent ChR2 expression in CeA. **(c)** Schematic representation of retro-cre in DMS and cre-dependent ChR2 expression in CeA for all subjects. **(d)** Procedure schematic. We used blue light (473 nm, 10 mW, 20 Hz, 25-ms pulse width, 2 s) to stimulate CeA→DMS neurons during the collection of each earned reward in mice without a history of stress. Valued state = prefed on untrained food-pellet type to control for general satiety. Devalued state = prefed on trained food-pellet type to induce sensory-specific satiety devaluation. **(e)** Press rates across training. Training: $F_{(1.85, 38.75)}$ = 62.18, $P < 0.0001$; Virus: $F_{(1, 21)}$ = 0.23, P = 0.64; Training x Virus: $F_{(3, 63)}$ = 0.05, P = 0.98. **(f)** Press rate during the subsequent devaluation probe test immediately following sensory-specific satiety on the trained pellet (Devalued condition) or an alternate pellet type (Valued condition). Value: $F_{(1, 21)}$ = 20.32, P = 0.0002; Virus: $F_{(1,21)}$ = 0.92, P = 0.35; Virus x Value: $F_{(1, 21)}$ = 1.17, P = 0.29. **(g)** Devaluation index. $t_{(21)}$ = 1.37, P = 0.19. GFP N = 17 (9 male), ChR2 N = 6 (3 male). Optogenetic activation of CeA→DMS projections at reward during learning neither affects affect acquisition of the lever-press behavior, nor the action-outcome learning needed to support flexible goal-directed behavioral control during the devaluation test.

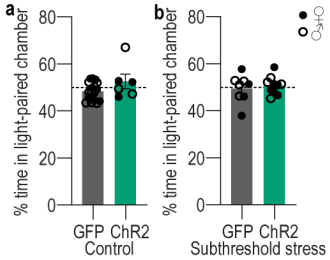

Supplemental Figure 4-4: Activation of CeA→DMS projections is neither rewarding or aversive. Following training and testing (Figure 4-3 and Figure 4o-u) mice receive a real-time place preference test in which 1 side of a 2-chamber apparatus was paired with optogenetic stimulation of DMS-projecting CeA neurons. **(a)** Average percent time spent in light paired chamber across 2, 10-minute sessions (one with light paired with each side) in handled control subjects. $t_{(21)} = 1.75$, $P = 0.10$. GFP N = 17 (9 male), ChR2 N = 6 (3 male). **(b)** Average percent time spent in light paired chamber across 2, 10-minute sessions (one with light paired with each side) in subjects with a prior once/daily CUS for 14 d. $t_{(16)} = 0.52$, $P = 0.61$. GFP N = 8 (4 male), ChR2 N = 10 (6 male). Males = closed circles, Females = open circles.

		Body Weight		
		Training Start	Training End	Statistics
Figure 1	Control	21.67 ± 0.82	21.54 ± 0.90	Stress x Time: $F_{(1, 45)}$ = 0.08, *P*= 0.77; Stress: $F_{(1, 45)}$ = 0.60, *P*= 0.44; Time: $F_{(1, 45)}$ = 1.79, *P*= 0.19
	Stress	20.79 ± 0.81	20.60 ± 0.82	
Figure 3	Control CeA	20.06 ± 0.94	20.24 + 0.71	Stress x Training: $F_{(1, 20)}$ = 0.16, P= 0.70; Stress: $F_{(1, 20)}$ = 1.02, P= 0.32; Training: $F_{(1, 20)}$ = 0.11, P= 0.75
	Stress CeA	19.12 ± 0.60	19.10 + 0.72	
	Control BLA	20.54 ± 1.00	20.25 + 0.92	Stress x Training: $F_{(1, 19)}$ = 2.67, P= 0.12; Stress: $F_{(1, 19)}$ = 2.24, P= 0.15; Training: $F_{(1, 19)}$ = 0.02, P= 0.88
	Stress BLA	18.66 ± 0.60	19.01 + 0.56	
Figure 4 top	Control mCherry	21.48 ± 1.01	21.08 ± 0.97	Group x Training: $F_{(2, 28)}$ = 0.20, P= 0.82; Group: $F_{(2, 28)}$ = 0.58, P= 0.57; Training: $F_{(1, 28)}$ = 1.57, P= 0.22
	Stress mCherry	20.65 ± 0.86	20.53 ± 0.97	
	Stress hM3Gq	20.06 ± 0.75	19.87 ± 0.72	
Figure 4-2	Control mCherry	21.48 ± 1.01	21.08 ± 0.97	Virus x Training: $F_{(1, 16)}$ = 2.00, P= 0.18; Virus: $F_{(1, 16)}$ = 0.45, P= 0.51; Training: $F_{(1, 16)}$ = 0.003, P= 0.96
	Control hM3Gq	19.91 ± 1.34	20.35 ± 1.64	
Figure 4 bottom	GFP	21.91 ± 1.30	21.25 ± 1.24	Virus x Training: $F_{(1, 19)}$ = 8.58, P= 0.009; Virus: $F_{(1, 19)}$ = 0.31, P= 0.59; Training: $F_{(1, 19)}$ = 4.96, P= 0.04
	Arch	20.73 ± 0.81	20.82 ± 0.75	
Figure 5 top	Control mCherry	21.81 ± 1.11	21.94 ± 1.11	Group x Training: $F_{(2, 29)}$ = 0.53, P= 0.59; Group: $F_{(2, 29)}$ = 0.08, P= 0.93; Training: $F_{(1, 29)}$ = 0.87, P= 0.36
	Stress mCherry	21.24 ± 1.03	21.66 ± 0.97	
	Stress hM4Gi	21.34 ± 1.08	21.30 ± 0.98	
Figure 5-2 top	Control mCherry	21.81 ± 1.11	21.94 ± 1.11	Virus x Training: $F_{(1, 23)}$ = 0.01, P= 0.92; Virus: $F_{(1, 23)}$ = 0.51, P= 0.48; Training: $F_{(1, 23)}$ = 0.44, P= 0.51
	Control hM4Gi	22.77 ± 0.90	22.96 ± 0.86	
Figure 5 middle	Control mCherry	21.44 ± 0.70	21.38 ± 0.79	Group x Training: $F_{(2, 20)}$ = 0.86, P= 0.44; Group: $F_{(2, 20)}$ = 1.02, P= 0.38; Training: $F_{(1, 20)}$ = 4.66, P= 0.04
	Stress mCherry	22.76 ± 0.99	22.03 ± 0.82	
	Stress Arch	21.00 ± 0.92	20.36 ± 0.92	
Figure 5-2 bottom	Control mCherry	21.44 ± 0.70	21.38 ± 0.79	Virus x Training: $F_{(1, 14)}$ = 0.15, P= 0.71; Virus: $F_{(1, 14)}$ = 0.70, P= 0.42; Training: $F_{(1, 14)}$ = 0.02, P= 0.90
	Control Arch	20.28 ± 1.03	20.31 ± 1.01	
Figure 5-3	Control GFP	20.87 ± 0.75	20.81 ± 0.70	Virus x Training: $F_{(1, 21)}$ = 0.79, P= 0.38; Virus: $F_{(1, 21)}$ = 0.94, P= 0.34; Training: $F_{(1, 21)}$ = 0.15, P= 0.70
	Control ChR2	19.34 ± 1.39	19.50 ± 1.4	
Figure 5 bottom	Sub-Stress GFP	19.33 ± 0.74	19.57 ± 0.73	Virus x Training: $F_{(1, 16)}$ = 4.55, P= 0.05; Virus: $F_{(1, 16)}$ = 1.73, P= 0.21; Training: $F_{(1, 16)}$ = 0.008, P= 0.93
	Sub-Stress ChR2	21.32 ± 1.04	21.05 ± 1.01	

Supplemental Table 1: Body weight across training. Values reflect average weight in grams ± s.e.m.

		Prefeed Consumption		
		Valued Outcome	Devalued Outcome	Statistics
Figure 1	Control	1.33 ± 0.09	1.32 ± 0.10	Stress x Value: $F_{(1, 45)} = 0.18$, $P = 0.67$; Stress: $F_{(1, 45)} = 0.13$, $P = 0.72$; Value: $F_{(1, 45)} = 0.33$, $P = 0.57$
	Stress	1.33 ± 0.08	1.25 ± 0.09	
Figure 4 top	Control mCherry	1.10 ± 0.68	1.39 ± 0.14	Group x Value: $F_{(2, 28)} = 3.93$, $P = 0.03$; Group: $F_{(2, 28)} = 1.51$, $P = 0.24$; Value: $F_{(1, 28)} = 0.70$, $P = 0.41$
	Stress mCherry	1.56 ± 0.13	1.28 ± 0.09	
	Stress hM3Gq	1.53 ± 0.10	1.23 ± 0.14	
Figure 4-2	Control mCherry	1.10 ± 0.68	1.39 ± 0.14	Virus x Value: $F_{(1, 16)} = 0.10$, $P = 0.76$; Virus: $F_{(1, 16)} = 0.83$, $P = 0.38$; Value: $F_{(1, 16)} = 3.50$, $P = 0.08$
	Control hM3Gq	1.27 ± 0.15	1.47 ± 0.17	
Figure 4 bottom	GFP	1.57 0.19	1.40 0.07	Virus x Value: $F_{(1, 19)} = 0.46$, $P = 0.50$; Virus: $F_{(1, 19)} = 0.007$, $P = 0.94$; Value: $F_{(1, 19)} = 0.21$, $P = 0.65$
	Arch	1.48 0.19	1.51 0.16	
Figure 5 top	Control mCherry	0.72 ± 0.13	0.80 ± 0.13	Group x Value: $F_{(2, 29)} = 0.62$, $P = 0.54$; Group: $F_{(2, 29)} = 1.13$, $P = 0.34$; Value: $F_{(1, 29)} = 0.17$, $P = 0.68$
	Stress mCherry	0.57 ± 0.16	0.54 ± 0.12	
	Stress hM4Gi	0.80 ± 0.14	0.79 ± 0.14	
Figure 5-2 top	Control mCherry	0.72 ± 0.13	0.80 ± 0.13	Virus x Value: $F_{(1, 23)} = 0.34$, $P = 0.57$; Virus: $F_{(1, 23)} = 0.04$, $P = 0.85$; Value: $F_{(1, 23)} = 0.20$, $P = 0.66$
	Control hM4Gi	0.69 ± 0.07	0.53 ± 0.13	
Figure 5 middle	Control mCherry	1.76 ± 0.16	1.64 ± 0.14	Group x Value: $F_{(2, 20)} = 0.91$, $P = 0.42$; Group: $F_{(2, 20)} = 2.66$, $P = 0.09$; Value: $F_{(1, 20)} = 0.007$, $P = 0.93$
	Stress mCherry	1.49 ± 0.14	1.70 ± 0.17	
	Stress Arch	1.42 ± 0.16	1.31 ± 0.10	
Figure 5-2 bottom	Control mCherry	1.76 ± 0.16	1.64 ± 0.14	Virus x Value: $F_{(1, 14)} = 1.28$, $P = 0.28$; Virus: $F_{(1, 14)} = 3.75$, $P = 0.07$; Value: $F_{(1, 14)} = 0.15$, $P = 0.70$
	Control Arch	1.38 ± 0.12	1.61 ± 0.13	
Figure 5-3	Control GFP	1.31 ± 0.09	1.47 ± 0.12	Virus x Value: $F_{(1, 25)} = 0.016$, $P = 0.90$; Virus: $F_{(1, 25)} = 0.24$, $P = 0.63$; Value: $F_{(1, 25)} = 1.96$, $P = 0.17$
	Control ChR2	1.36 ± 0.16	1.55 ± 0.15	
Figure 5 bottom	Sub-Stress GFP	1.56 ± 0.21	1.53 ± 0.15	Virus x Value: $F_{(1, 16)} = 0.09$, $P = 0.77$; Virus: $F_{(1, 16)} = 1.22$, $P = 0.29$; Value: $F_{(1, 16)} = 0.01$, $P = 0.92$
	Sub-Stress ChR2	1.68 ± 0.15	1.75 ± 0.14	

Supplemental Table 2: Sensory-specific satiety prefeed consumption. Values reflect average amount consumed in grams ± s.e.m.

		Average Choice Consumption		
		Valued Outcome	Devalued Outcome	Statistics
Figure 1	Control	0.25 ± 0.03	0.01 ± 0.01	Stress x Value: $F_{(1, 26)} = 0.002$, $P = 0.97$; Stress: $F_{(1, 26)} = 0.006$, $P = 0.94$; Value: $F_{(1, 26)} = 132.10$, $P < 0.0001$
	Stress	0.25 ± 0.03	0.01 ± 0.01	
Figure 4 top	Control mCherry	0.23 ± 0.01	0.01 ± 0.01	Group x Value: $F_{(2, 28)} = 1.28$, $P = 0.29$; Group: $F_{(2, 28)} = 3.81$, $P = 0.03$; Value: $F_{(1, 28)} = 248.30$, $P < 0.0001$
	Stress mCherry	0.29 ± 0.03	0.02 ± 0.01	
	Stress hM3Gq	0.24 ± 0.02	0.01 ± 0.01	
Figure 4-2	Control mCherry	0.23 ± 0.01	0.01 ± 0.01	Virus x Value: $F_{(1, 16)} = 0.82$, $P = 0.38$; Virus: $F_{(1, 16)} = 1.63$ $P = 0.22$; Value: $F_{(1, 16)} = 229.10$, $P < 0.0001$
	Control hM3Gq	0.24 ± 0.02	0.04 ± 0.03	
Figure 4 bottom	GFP	0.25 0.03	0.02 0.01	Virus x Value: $F_{(1, 19)} = 0.14$, $P = 0.71$; Virus: $F_{(1, 19)} = 1.21$, $P = 0.29$; Value: $F_{(1, 19)} = 118.00$, $P < 0.0001$
	Arch	0.30 0.04	0.05 0.02	
Figure 5 top	Control mCherry	0.16 ± 0.04	0.11 ± 0.04	Group x Value: $F_{(2, 29)} = 0.32$, $P = 0.73$; Group: $F_{(2, 29)} = 0.60$, $P = 0.55$; Value: $F_{(1, 29)} = 2.25$, $P = 0.14$
	Stress mCherry	0.12 ± 0.04	0.10 ± 0.04	
	Stress hM4Gi	0.21 ± 0.06	0.14 ± 0.04	
Figure 5-2 top	Control mCherry	0.16 ± 0.04	0.11 ± 0.04	Virus x Value: $F_{(1, 23)} = 0.03$, $P = 0.87$; Virus: $F_{(1, 23)} = 0.37$, $P = 0.55$; Value: $F_{(1, 23)} = 4.19$, $P = 0.0522$
	Control hM4Gi	0.19 ± 0.05	0.16 ± 0.06	
Figure 5 middle	Control mCherry	0.27 ± 0.04	0.02 ± 0.01	GrouP x Value: $F_{(2, 20)} = 2.40$, $P = 0.12$; Group: $F_{(2, 20)} = 2.90$, $P = 0.08$; Value: $F_{(1, 20)} = 108.20$, $P < 0.0001$
	Stress mCherry	0.21 ± 0.03	0.02 ± 0.01	
	Stress Arch	0.16 ± 0.02	0.01 ± 0.01	
Figure 5-2 bottom	Control mCherry	0.27 ± 0.04	0.02 ± 0.01	Virus x Value: $F_{(1, 14)} = 0.63$, $P = 0.44$; Virus: $F_{(1, 14)} = 1.45$, $P = 0.25$; Value: $F_{(1, 14)} = 66.50$, $P < 0.0001$
	Control Arch	0.21 ± 0.03	0.01 ± 0.01	
Figure 5-3	Control GFP	0.27 ± 0.02	0.02 ± 0.01	Virus x Value: $F_{(1, 25)} = 0.001$, $P = 0.97$; Virus: $F_{(1, 25)} = 0.22$, $P = 0.64$; Value: $F_{(1, 25)} = 160.50$, $P < 0.0001$
	Control ChR2	0.28 ± 0.03	0.02 ± 0.01	
Figure 5 bottom	Sub-Stress GFP	0.27 ± 0.03	0 ± 0.01	Virus x Value: $F_{(1, 16)} = 0.18$, $P = 0.68$; Virus: $F_{(1, 16)} = 0.001$, $P = 0.98$; Value: $F_{(1, 16)} = 211.40$, $P < 0.0001$
	Sub-Stress ChR2	0.26 ± 0.02	0 ± 0.01	

Supplemental Table 3: Average post-probe-test choice consumption. Values reflect average amount consumed in grams ± s.e.m.

	Statistics on log transformed normalized data
Figure 1d	Training: $F_{(2.19, 98.33)} = 230.7$, $P < 0.0001$; Stress: $F_{(1, 45)} = 1.50$, $P = 0.23$; Training x Stress: $F_{(3, 135)} = 2.62$, $P = 0.05$
Figure 1e	Value x Stress: $F_{(1, 45)} = 6.80$, $P = 0.01$; Value: $F_{(1, 45)} = 3.25$, $P = 0.08$; Stress: $F_{(1, 45)} = 2.74$, $P = 0.01$
Figure 1-1a	$t_{(22)} = 0.25$, $P = 0.81$
Figure 1-1g	$t_{(22)} = 1.05$, $P = 0.30$
Figure 1-1h	$t_{(22)} = 1.66$, $P = 0.11$
Figure 1-1j	Sucrose: $F_{(1, 22)} = 251.6$, $P < 0.0001$; Stress: $F_{(1, 22)} = 1.88$, $P = 0.18$; Sucrose x Stress: $F_{(1, 22)} = 0.17$, $P = 0.68$
Figure 1-2b	Stress x Value: $F_{(1, 45)} = 6.76$, $P = 0.01$; Value: $F_{(1, 45)} = 4.05$, $P = 0.05$; Stress: $F_{(1, 45)} = 0.14$, $P = 0.71$
Figure 3e	Training: $F_{(2.86, 54.35)} = 140.8$, $P < 0.0001$; Stress: $F_{(1, 19)} = 1.36$, $P = 0.26$ Training x Stress: $F_{(3, 57)} = 0.76$, $P = 0.52$
Figure 3k	Training: $F_{(2.34, 46.85)} = 110.9$, $P < 0.0001$; Stress: $F_{(1, 20)} = 0.65$, $P = 0.43$; Training x Stress: $F_{(3, 60)} = 0.12$, $P = 0.95$
Figure 3-1a	Training: $F_{(2.81, 53.39)} = 1.07$, $P = 0.037$; Stress: $F_{(1, 19)} = 0.23$, $P = 0.64$; Training x Stress: $F_{(3, 57)} = 0.17$, $P = 0.91$
Figure 3-1b	Training: $F_{(2.50, 49.98)} = 1.20$, $P = 0.32$; Stress: $F_{(1, 20)} = 2.82$, $P = 0.11$; Training x Stress: $F_{(3, 60)} = 0.23$, $P = 0.87$
Figure 3-3a	Training: $F_{(2.41, 45.76)} = 0.28$, $P = 0.80$; Stress: $F_{(1, 19)} = 0.08$, $P = 0.79$; Training x Stress: $F_{(3, 57)} = 1.29$, $P = 0.29$
Figure 3-3b	Training: $F_{(2.50, 47.58)} = 0.62$, $P = 0.58$; Stress: $F_{(1, 19)} = 0.01$, $P = 0.93$; Training x Stress: $F_{(3, 57)} = 1.39$, $P = 0.26$
Figure 3-3c	Training: $F_{(2.50, 50.01)} = 0.31$, $P = 0.78$; Stress: $F_{(1, 20)} = 2.77$, $P = 0.11$; Training x Stress: $F_{(3, 60)} = 0.82$, $P = 0.49$
Figure 3-3d	Training: $F_{(2.68, 53.58)} = 0.34$; $P = 0.71$; Stress: $F_{(1, 20)} = 3.75$, $P = 0.07$; Training x Stress: $F_{(3, 60)} = 0.49$, $P = 0.69$
Figure 4e	Training: $F_{(2.08, 58.34)} = 122.3$, $P < 0.0001$; Group: $F_{(2, 28)} = 0.28$, $P = 0.76$; Training x Group: $F_{(6, 84)} = 0.74$, $P = 0.62$
Figure 4f	Value: $F_{(1, 28)} = 24.00$, $P < 0.0001$; Group: $F_{(2, 28)} = 1.91$, $P = 0.17$; Value x Group: $F_{(2, 28)} = 3.25$, $P = 0.05$
Figure 4l	Training: $F_{(2.13, 40.54)} = 66.41$, $P < 0.0001$; Virus: $F_{(1, 19)} = 1.13$, $P = 0.30$; Training x Virus: $F_{(3, 57)} = 0.89$, $P = 0.45$
Figure 4m	Virus x Value: $F_{(1, 19)} = 13.52$, $P = 0.002$; Virus: $F_{(1, 19)} = 0.40$, $P = 0.54$; Value: $F_{(1, 19)} = 0.17$, $P = 0.68$
Figure 4-1c	Value x Virus: $F_{(1, 16)} = 6.67$, $P = 0.02$; Value: $F_{(1, 16)} = 8.56$, $P = 0.01$; Virus: $F_{(1, 16)} = 2.43$, $P = 0.14$
Figure 4-1e	Value: $F_{(1, 16)} = 4.37$, $P = 0.05$; Virus: $F_{(1, 16)} = 1.02$, $P = 0.33$; Value x Virus: $F_{(1, 16)} = 0.65$, $P = 0.43$
Figure 4-2b	Value: $F_{(1, 28)} = 11.03$, $P = 0.002$; Group: $F_{(2, 28)} = 2.39$; $P = 0.11$; Group x Value: $F_{(2, 28)} = 1.70$, $P = 0.20$
Figure 4-2d	Value: $F_{(1, 19)} = 5.89$, $P = 0.03$; Virus: $F_{(1, 19)} = 0.47$, $P = 0.50$; Virus x Value: $F_{(1, 19)} = 0.14$, $P = 0.71$
Figure 4-3	$t_{(19)} = 0.60$, $P = 0.55$
Figure 5e	Training: $F_{(2.17, 62.90)} = 25.48$, $P < 0.0001$; Group: $F_{(2, 29)} = 0.17$, $P = 0.85$; Training x Group: $F_{(6, 87)} = 1.19$, $P = 0.32$
Figure 5f	Value: $F_{(1, 29)} = 16.02$, $P = 0.0004$; Group: $F_{(2, 29)} = 3.26$; $P = 0.05$; Group x Value: $F_{(2, 29)} = 3.29$, $P = 0.05$
Figure 5g	$F_{(2, 29)} = 0.22$, $P = 0.07$
Figure 5l	Training: $F_{(2.88, 57.64)} = 70.40$, $P < 0.0001$; Group: $F_{(2, 20)} = 0.79$, $P = 0.47$; Training x Group: $F_{(6, 60)} = 1.36$, $P = 0.25$
Figure 5m	Value x Group: $F_{(2, 20)} = 7.40$, $P = 0.004$; Group: $F_{(1, 20)} = 7.53$, $P = 0.01$; Value: $F_{(2, 20)} = 2.55$, $P = 0.10$
Figure 5s	Training: $F_{(3, 48)} = 115.0$, $P < 0.0001$; Virus: $F_{(1, 16)} = 0.03$, $P = 0.87$; Training x Virus: $F_{(3, 48)} = 0.15$, $P = 0.93$
Figure 5t	Virus x Value: $F_{(1, 16)} = 8.36$, $P = 0.01$; Virus: $F_{(1, 16)} = 0.57$, $P = 0.46$; Value: $F_{(1, 16)} = 0.81$, $P = 0.38$
Figure 5-1a	Training: $F_{(2.36, 54.33)} = 33.34$, $P < 0.0001$; Virus: $F_{(1, 23)} = 0.22$, $P = 0.65$; Training x Virus: $F_{(3, 69)} = 0.29$, $P = 0.84$
Figure 5-1b	Training: $F_{(1.95, 44.91)} = 3.29$, $P = 0.05$; Virus: $F_{(1, 23)} = 0.35$, $P = 0.56$; Training x Virus: $F_{(3, 69)} = 0.44$, $P = 0.73$
Figure 5-1c	Virus: $F_{(1, 23)} = 10.54$, $P = 0.004$; Value: $F_{(1, 23)} = 0.98$, $P = 0.33$; Value x Virus: $F_{(1, 23)} = 1.42$, $P = 0.24$
Figure 5-1d	$t_{(23)} = 0.86$, $P = 0.40$
Figure 5-1f	Training: $F_{(2.46, 34.50)} = 21.85$, $P < 0.0001$; Virus: $F_{(1, 14)} = 0.67$, $P = 0.43$; Training x Virus: $F_{(3, 42)} = 0.21$, $P = 0.89$
Figure 5-1g	Training: $F_{(3, 42)} = 0.53$, $P = 0.66$; Virus: $F_{(1, 14)} = 3.43$, $P = 0.09$; Training x Virus: $F_{(3, 42)} = 1.77$, $P = 0.17$
Figure 5-1h	Value: $F_{(1, 14)} = 7.68$, $P = 0.02$; Virus: $F_{(1, 14)} = 1.07$, $P = 0.32$; Value x Virus: $F_{(1, 14)} = 0.02$. $P = 0.90$
Figure 5-1j	Value: $F_{(1, 14)} = 3.10$, $P = 0.10$; Virus: $F_{(1, 14)} = 0.44$, $P = 0.52$; Value x Virus: $F_{(1, 14)} = 0.69$, $P = 0.42$
Figure 5-2b	Value: $F_{(1, 30)} = 5.85$, $P = 0.02$; Group: $F_{(2, 30)} = 0.59$, $P = 0.56$; Group x Value: $F_{(2, 30)} = 0.83$, $P = 0.44$

Figure 5-2c	Training x Group: $F_{(6, 60)} = 2.65$, $P = 0.02$; Training: $F_{(2.33, 46.66)} = 1.78$, $P = 0.17$; Group: $F_{(2, 20)} = 1.38$, $P = 0.27$
Figure 5-2d	Value: $F_{(1, 20)} = 3.38$, $P = 0.08$; Group: $F_{(2, 20)} = 0.43$, $P = 0.66$; Group x Value: $F_{(2, 20)} = 1.36$, $P = 0.28$
Figure 5-2e	Training: $F_{(2.21, 46.33)} = 1.38$, $P = 0.26$; Virus: $F_{(1, 21)} = 2.50$, $P = 0.13$; Training x Virus: $F_{(3, 63)} = 0.09$, $P = 0.97$
Figure 5-2h	Value: $F_{(1, 16)} = 2.65$, $P = 0.12$; Virus: $F_{(1, 16)} = 0.71$, $P = 0.41$; Value x Virus: $F_{(1, 16)} = 0.74$, $P = 0.40$
Figure 5-3e	Training: $F_{(1.57, 33.00)} = 73.47$, $P < 0.0001$; Virus: $F(1, 21) = 0.005$, $P = 0.94$; Training x Virus: $F_{(3, 63)} = 0.80$, $P = 0.50$
Figure 5-3f	Value: $F_{(1, 21)} = 7.64$, $P = 0.01$; Virus: $F_{(1, 21)} = 0.36$, $P = 0.55$; Virus x Value: $F_{(1, 21)} = 0.36$, $P = 0.56$
Figure 5-3g	$t_{(20)} = 2.39$; $P = 0.03$

Supplemental Table 4: Statistical supplement for log-transformed normalized datasets.

Category	Item	Vendor	Catalog #	Lot #	Titer
ELISA Kit	Highly sensitive corticosterone ELISA kit	Enzo Life Sciences	ADI-900-097	02252009C	
Viruses/Tracers	AAV8-hSyn-mCherry	UNC Vector Core	114472	v113707	2.6 x 10^{13} gc/mL
	Fluorogold	Santa Cruz Biotechnology	sc-358883	A1223	
	AAV9-Syn-FLEX-jGCaMP8s-WPRE	Addgene	162377	v118930	5 x 10^{12} gc/mL
	AAVrg-hSyn-Cre-P2A-tdTomato	Addgene	107738	v75881	1.5 x 10^{13} pp/mL
	AAV2-hSyn-DIO-hM3D(Gq)-mCherry	Addgene	44361	v97910	2.0 x 10^{13} gc/mL
	AAV2-hSyn-DIO-hM4D(Gi)-mCherry	Addgene	44362	v68359	1.5 x 10^{13} gc/mL
	AAV2-hSyn-DIO-mCherry	Addgene	50459	v107704	1.6 x 10^{13} gc/mL
	AAV2-hSyn-DIO-mCherry	Addgene	50459	v54505	1.8 x 10^{13} gc/mL
	AAV2-hSyn-DIO-mCherry	Addgene	50459	v122065	2.1 x 10^{13} gc/mL
	AAV8-hSyn-GFP	Addgene	50465	v53294	2.5 x 10^{13} pp/mL
	AAV8-hSyn-DIO-eYFP	Stanford Vector Core	GVVC-AAV-206	7463	1 x 10^{13} vg/mL
	AAV8-hSyn-DIO-ChR2-eYFP	Stanford Vector Core	GVVC-AAV-207	7464	7.5 x 10^{12} vg/mL
	AAV-DJ-hSyn-eArch-eYFP	Stanford Vector Core	GVVC-AAV-146	4799	1 x 10^{13} gc/mL
	AAV-DJ-hSyn-eArch-eYFP	Stanford Vector Core	GVVC-AAV-146	5105	9.3 x 10^{12} gc/mL
	CAV2-Cre-GFP	Plateforme de Vectorologie de Montpellier	N/A	N/A	1.42 x 10^{13} pp/mL
	CAV2-Cre-GFP	Plateforme de Vectorologie de Montpellier	N/A	N/A	9.6 x 10^{12} pp/mL
	AAV8-hSyn-FLEX-TVA-P2A-GFP-2A-oG	Salk Vector Core	85225	N/A	2.53 x 10^{12} gc/mL
	AAV8-hSyn-FLEX-TVA-P2A-GFP-2A-oG	Salk Vector Core	85225	N/A	1.87 x 10^{12} gc/mL
	EnvA-Gdeleted-Rabies-mCherry	Salk Vector Core	32636	N/A	1.0 x 10^{8} TU/mL
Antibodies	Chicken polyclonal anti-mCherry primary antibody	Abcam	ab205402	GR3368071-2, GR3271744-8	
	Chicken polyclonal anti-GFP primary antibody	Abcam	ab13970	1018753-7, 1018753-5, 1018753-11, 1018753-12	
	Living Colors Rabbit DsRed Polyclonal Antibody	Takara Bio	632496	1904182, 2210019	
	Goat anti-Rabbit IgG Secondary Antibody, Alexa Fluor 594	Invitrogen	A11012	2433881, 2119134	
	Goat anti-Chicken IgY Secondary Antibody, Alexa Fluor 488	Abcam	ab150169	GR3437715-3	

Supplemental Table 5: Key reagents information.